ISME

Iranian Journal of Mechanical Engineering
The Iranian Society of Mechanical Engineers
Research Paper

DOI: 10.30506/JMEE.2022.550895.1286
DOR: 20.1001.1.16059727.2022.23.2.7.6

E. Kouhi*
Ph.D. Candidate

A. Bak Khoshnevis†
Professor

Experimental Investigation of the Flow Structure around a Pitching Airfoil by Mean and Instantaneous Data

This paper focuses on a selected set of results from extensive experimental tests to characterize the wake aerodynamics of an SD7062 wind turbine airfoil in steady-state and pitch oscillating motion. Investigating the wake of an airfoil provides outstanding information on physical aspects of the downstream. Wake measurements were accomplished through hot-wire anemometers in the Laboratory of Aerodynamics at the Hakim Sabzevari University. The impact of AoA and Reynolds number were both examined in the steady-state. Regarding the pitching airfoil motion, the effect of reduced frequency, Reynolds number, symmetric, and asymmetric oscillation were also investigated. The results revealed that in both the pitching and the steady-state cases, strength of the vortices is highly related to the airfoil shape, amplitude, and Reynolds number. In respect of pitching state, the TI value is decreased as the Reynolds number increases, while it grows up with increasing the reduced frequency. Besides, TI in asymmetry oscillation is significantly higher than in symmetric oscillation, which is probably due to the formation of larger vortices. For steady-state, the instantaneous TI and velocity are almost the same as their mean values. Hence, statistical data could be used to calculate aerodynamic forces on a static airfoil. It is necessary to meticulously consider the effect of mean and instantaneous forces in the pitching state, as the forces acting on the pitching airfoil could reach several times its average state in some moments during its impact. As a result, the importance of these instantaneous loads is required to be considered enabling us to select the proper material for the airfoil.

Keywords: Wind tunnel, Pitching airfoil, Hot-wire, Aerodynamic forces, Experimental investigation.

1 Introduction

Extensive works have been conducted on unsteady flows, specifically flows passing through oscillating airfoils for nearly a century due to their application and complexity. Among these

*Ph.D. Candidate, Department of Mechanical Engineering, Hakim Sabzevari University, Sabzevar, Iran

†Corresponding Author, Professor, Department of Mechanical Engineering, Hakim Sabzevari University, Sabzevar, Iran

Receive: 2022/03/22 Accepted: 2022/07/09

applications, investigating the loads applied to helicopter blades [1-3], submarine blades [4,5], and turbomachine blades [6,7] are worth mentioning. Many other studies have been focused on the prediction and control of vibration of flying objects and missiles [8] as well as the prediction of fixed dynamic properties in modern flying objects and missiles [9]. Also, a long list of applications, namely the vibration of hydrofoils due to cavitation phenomenon [10], wind turbine blade [11,12], the aerodynamic efficiency of oscillating wings in birds [13,14], zoological studies in the field of animals that can produce high lifting force [15], and far more others were also reviewed. However, the underlying mechanism of unsteady flow through oscillating airfoils is still incomplete and unknown due to its complexity. Understanding the details of this mechanism opens up new horizons for modern applications motivating researchers in this field to take this long way.

In recent years, horizontal axis wind turbines (HAWTs) have been the predominant technology used by wind farms [16]. Flow around HAWT airfoil, also known as "pitching airfoil flow", is an unsteady phenomenon that can be analyzed by experimental and numerical methods. The first step to understanding the phenomenon of pitching airfoil flow is to identify the factors affecting this type of flow. Previous researchers have revealed that the characteristics of the near wake of oscillatory airfoils are highly influenced by mean incidence, reduced frequency, the amplitude of oscillation, and airfoil shapes, each of which affects the trailing-edge vortex [17, 18]. Aerodynamic loads can be predicted by the wake survey method, which means investigating the wake of a pitching airfoil can provide valuable information about its flow characteristics. The following represents some literature including experimental and numerical findings using the airfoil wake survey method.

Ma et al. [19] investigated the unsteady lift of a pitching airfoil encountering a sinusoidal stream-wise gust. They used two-dimensional pitch oscillating airfoil with a NACA0015 profile. They represented that the experimental results agree with Greenberg's prediction with a slight deviation. Zhu et al. [20] carried out an experimental investigation of Isaacs' incompressible unsteady airfoil theory in the context of the trailing edge flow under an oscillating freestream. They used elliptical choke vanes to generate time-varying freestream velocity. They observed that the effects of velocity amplitude and reduced frequency on the lift response are similar to what is predicted in Isaacs' theory but with significant differences in the magnitude of the lift overshoot and undershoot and corresponding phases. Tabrizian et al. [21] conducted an experimental study on boundary-layer transition detection over a supercritical pitching airfoil using hot-film sensors. They showed that the formation of a laminar separation bubble near the leading edge and at relatively higher AoAs leads to the transition of the boundary layer. It was also observed that increasing the reduced frequency leads to a delay in transition onset, postponing it to a higher AoA, widening the hysteresis between the upstroke and downstroke motions. Wernert et al. [22] experimentally investigated the dynamic stall process on a NACA 0012 using PIV and laser-sheet detection measurement methods. The Reynolds number and the reduced frequency were considered 3.73×10^5 and 0.15, respectively, and the airfoil motion range was between 5 and 25 degrees. Four main phases of the dynamic stall process, including attached flow, post-stall vortex shedding, dynamic stall vortex development, and reattachment, were compared between numerical and experimental approaches. Soltani and Mahmoudi [23] assessed the unsteady wake behavior behind a pitching airfoil which was a section of a wind turbine blade. In a wind tunnel, the effect of various reduced frequencies, amplitudes, and mean AoAs were obtained on instantaneous and mean velocity profiles. They compared the oscillation cycle with static airfoil data in real-time and average variations of the linear momentum deficit. An investigation of the average AoA effects on the velocity profiles and aerodynamic coefficient were performed as well. Their findings confirmed that the amplitude and frequency of the oscillation have a significant impact on the aerodynamic coefficients. Anderson et al. [24] considered thrust-producing on harmonically oscillating airfoils. They classified the principal characteristics of the flow around and in the

wake of a flapping NACA 0012 airfoil. They implied that high efficiency accompanied by significant thrust development is associated with the generation of moderately strong leading-edge vortices, which subsequently amalgamated with trailing-edge vorticity, leading to a reverse Karman street. Chang [25] tested the Reynolds-number effects in the near-wake region of an oscillating NACA 4412 and discussed the instantaneous velocity field and the TI in the near-wake region at different Reynolds numbers. Satyanarayana [26] focused on the unsteady characteristics of airfoils and cascades at low-frequency parameters. Unsteady pressures, wakes, and boundary layers measured in sinusoidal flow. He obtained time-mean and time-dependent wake profiles of an airfoil and in cascades airfoils and compared the unsteady wake losses from time-mean wake profiles. The experimental results were compared to the predicted unsteady pressure distribution on an airfoil, presenting unsteady pressure differentials near the trailing-edge region. Moreover, Mamouri et al. [27] experimentally investigated the effective parameters on the offshore wind turbine pitching airfoil. They evaluated the aerodynamic coefficients of a pitch oscillating wind turbine airfoil. They studied the effect of reduced frequency, mean AoA, amplitude, and Reynolds number on hysteresis loops. Koochesfahani [28] explored vortical patterns in the wake of a pitching airfoil. Goodman et al. [29] studied the near wake turbulent flow properties of the SD7003 airfoil. Boroumand and Mani [30] measured root-mean-square, correlation, mean value distribution, time history, and frequency of the wake of pitch oscillating supercritical airfoil in compressible flow using hot-wire. Masdari and et al. [31] had a series of experimental tests to present lift characteristics of a pitching wind turbine airfoil at near and post-stall regions. They showed that increasing the reduced frequency leads to a delay in maximum lift occurrence and a decrease in lift curve slope. They also disclosed that the mean AoA and amplitude of pitching motion affect lift. They indicated that increasing the amplitude makes the airfoil enter the post-stall region and delays the maximum lift occurrence, and encounters deeper dynamic stall as well. Gisbert et al. [32] studied the impacts of Reynolds number and reduced frequency on low-pressure turbine airfoils both numerically and experimentally. They tested three Reynolds numbers and two reduced frequencies on a low pressure turbine using hot-wire, Laser Doppler Velocimetry (LDV) and pressure tapings. Castillo and Pol [33] presented a wind tunnel case study to explore the effect of combining yaw-based wake steering on the wake trajectory. The wake oscillations as a result of wind direction, changed sinusoidally yawing the turbine. Hot-wire and Particle Image Velocimetry (PIV) methods were used for gathering the measurements. Yadegari and Khoshnevis [34] investigated the effect of trip wire on the wake characteristics of a smooth elliptic cylinder at a zero angle of attack. In their experiment, hot-wire anemometer was used for measuring instantaneous fluid flow velocity in the wake. They exposed that the wire has a significant effect on flow characteristics and reduction in the drag coefficient, and furthermore, this influence strongly depends on the location where the trip wire is installed on the model. Yang et al.[35] conducted the aerodynamic characteristics of a pitching wind turbine airfoil with a Gurney flap under turbulent inflow. They carried out an offshore wind turbine airfoil under different turbulence levels at Reynolds number 105. They used surface pressure and near-wake flow field methods to measure the turbulence intensity and hysteresis loops of the wake. Aziz and Mukherjee [36] investigated vortex interaction and roll-up in unsteady flow past through airfoils. They used time-step to predict the individual wake shapes and modeled the unsteady wake by discrete vortices. Their results revealed a wide range of information about the effects of relative velocity, phase-lag, and pitching rate on airfoil performance. Mamouri et al. [37] performed an analysis of pitching airfoils for offshore wind turbines under a dynamic-stall condition. They simulated a 2D unsteady-state flow field across diverse oscillatory frequencies to observe the dynamic stall. They exhibited that S822 and SD7062 airfoils, associating a delay in flow separation, yield slightly lower drag coefficients compared with S809 airfoil. Kou and Zhang [38] studied multi-kernel neural networks for nonlinear unsteady aerodynamic reduced-order modeling. Results demonstrated that for unsteady or any nonlinear

dynamic systems, multi-kernel networks are the most suitable among machine trained network models.

In this paper, we are going to experimentally investigate the flow structures around a pitching wind turbine airfoil using hot-wire anemometer. To reach this aim, turbulence intensity and non-dimensional velocity are explored in static and pitching airfoil. The effect of four AoAs (zero, 11, -11, and 20), two different Reynolds numbers (about 150000 and 250000), and seven stations behind the airfoil are examined in the steady-state. In the pitching airfoil motion, the effect of reduced frequency, Reynolds number, symmetric AoAs (-10 to 10), and asymmetric AoAs (0 and 20) are also considered. It should be noted that while most of the previous studies have focused only on statistical data, the novelty of this research is considering both instantaneous and statistical hot-wire data to analyze the large variety of variable parameters such as Reynolds numbers, symmetry and asymmetry amplitudes, as well as different reduced frequencies in downstream stations. Investigating the velocity and TI profiles in the wake of an airfoil provides outstanding information on physical aspects of the downstream flow including the velocity defect, diffusion amplitude and maximum TI. These parameters are applicable in designing tandem airfoils such as wind turbines and helicopter propellers. For instance, having a grasp of the effect of front wind turbine blades on airflow helps us find the proper location for back wind turbines. Although statistical analysis of turbulence variables provides us with an overview of the phenomenon, in-depth information about the impact loads on the airfoil is merely accessible through instantaneous analysis.

2 Experimental Setup and Procedure

The experimental tests were carried out in a low-speed wind tunnel located in the Laboratory of Aerodynamics at Hakim Sabzevari University (HSU). It is an open-circuit wind tunnel with a square cross-section of 40 cm×40 cm and a test section length of 168 cm. The contraction ratio of the wind tunnel is 3:1. Figure (1) illustrates the schematic of this wind tunnel to gain a better insight on its structure.

The maximum freestream TI is less than 0.1% provided in figure (2a). The non-dimensional velocity profiles are plotted along the width of the test section provided in figure (2b). The maximum reachable free stream velocity inside the test section equals 30 m/s. The blockage ratio is %6 in AoA of zero. However, in all cases of AoAs, the blockage ratio is less than 10%, and the blockage yields appropriate results until it reaches 10%, as stated by [39, 40]. Therefore, no correction is required for the measured free stream velocity.

The selected airfoil in this experiment is SD7062, and the validation airfoil is NACA0012 (See figure (3)). The airfoils are made of Poly Lactic Acid by the 3D printing method; consequently, their surfaces are thoroughly polished and covered with resin.

Figure (4) presents the SD7062 airfoil, whereas table (1) tabulated the details of SD7062 and NACA0012 Airfoils. The airfoils oscillate around C/4 of the leading edge.

The pitching motion of the airfoils is shown by equation (1), where α is the instantaneous AoA, $\bar{\alpha}$ is mean AoA, f is the frequency of oscillation, and α_0 is pitch oscillation amplitude (See figure (5)).

$$\alpha = \bar{\alpha} + \alpha_0 \sin(2\pi ft) \tag{1}$$

The instantaneous AoAs varies from -10 to +10 degrees for symmetry and 0 to 20 degrees for asymmetry oscillation.

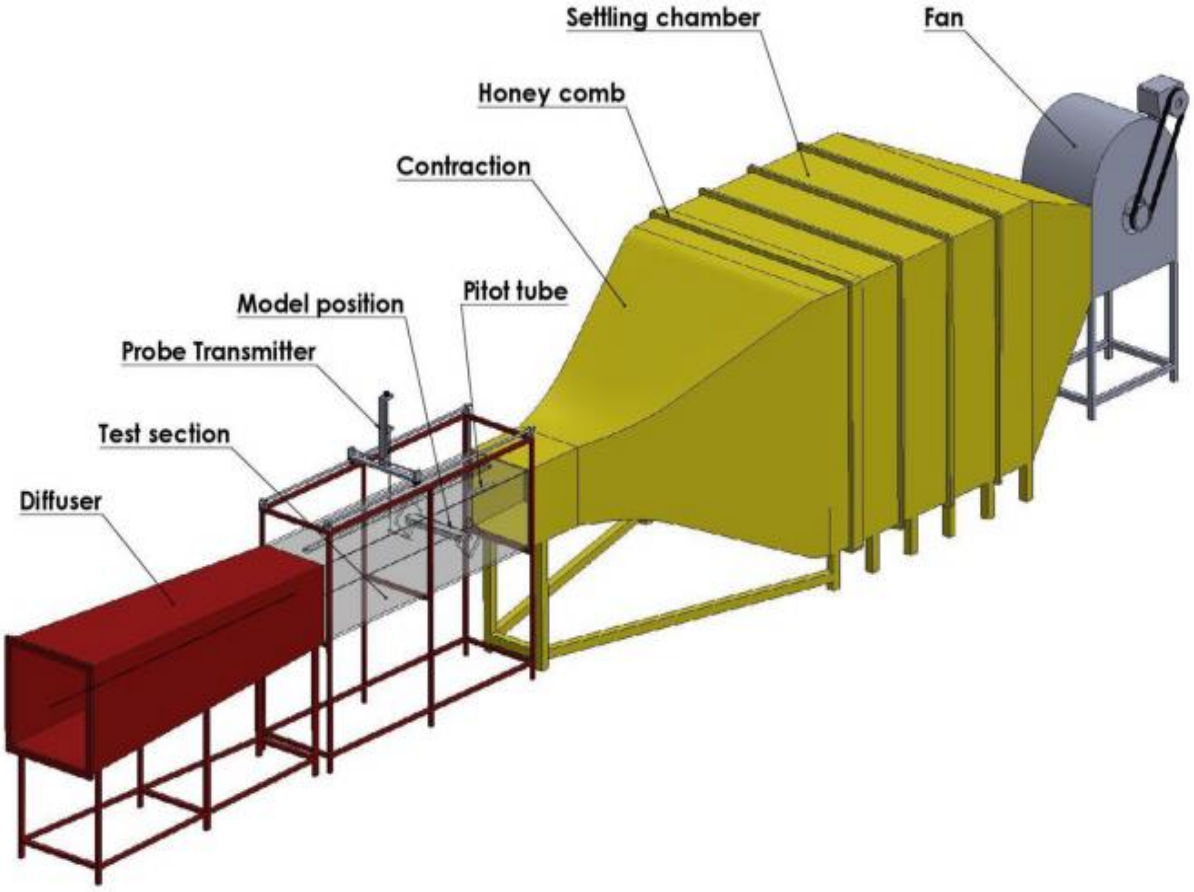

Figure 1 Schematic view of wind tunnel Laboratory of Aerodynamics at Hakim Sabzevari University

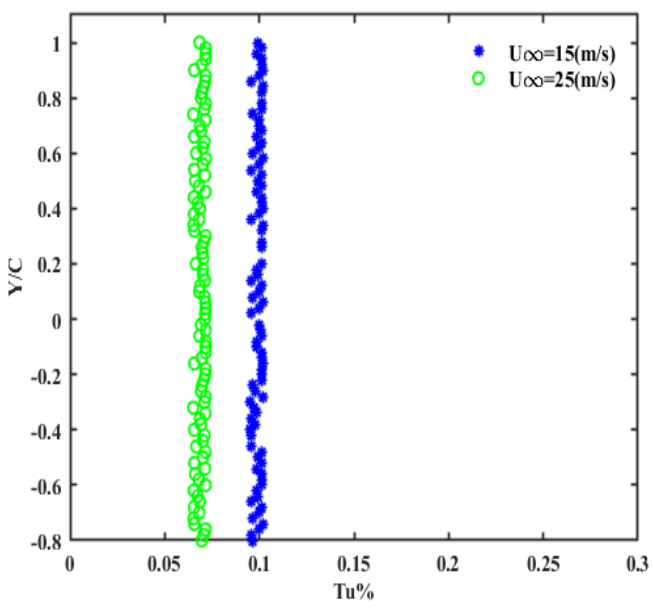

a) Turbulence intensity of free streamflow at the beginning of the test section

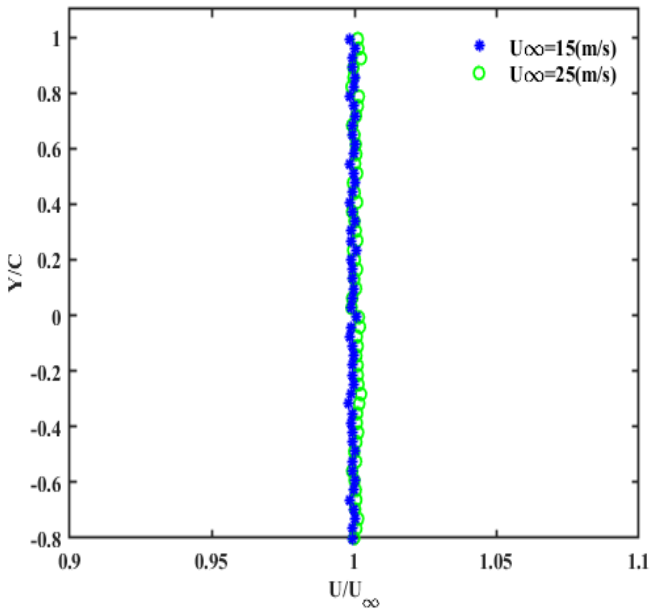

b) The non-dimensional velocity profile at the beginning of the test section

Figure 2 Investigating the entrance area to the test section of the wind tunnel

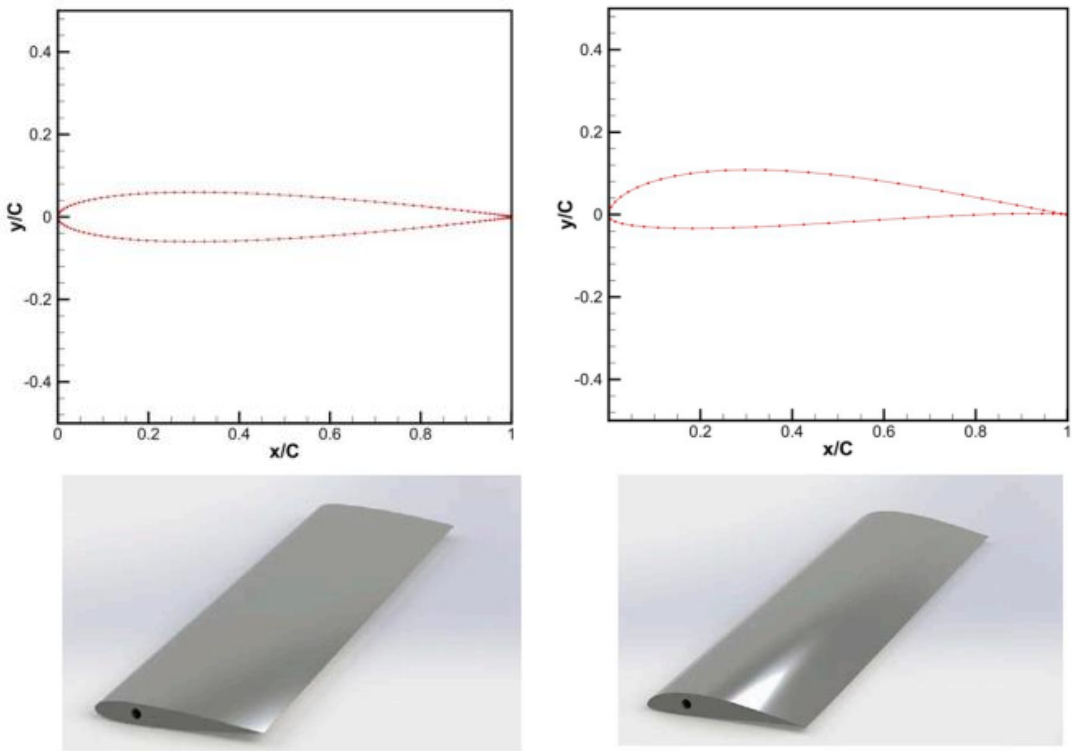

a) Validation airfoil (NACA0012) b)Tested airfoil (SD7062)

Figure 3 Validation (a) and tested (b) airfoils

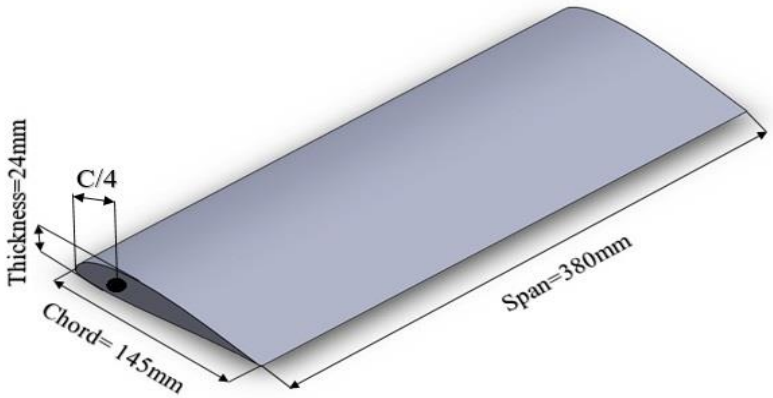

Figure 4 Details of SD7062 airfoil

Table 1 Details of the tested S7062 and NACA0012 Airfoils

Details	SD7062	NACA0012
Chord	145 mm	130 mm
Max thickness	16% at 39.2% chord	12% at 30% chord
Max chamber	1.8% at 59.5% chord	0% at 0% chord
Freestream Velocity	15 and 25 m/s	
Chord based Reynolds Number	Re_1=153169 and Re_2=255282	

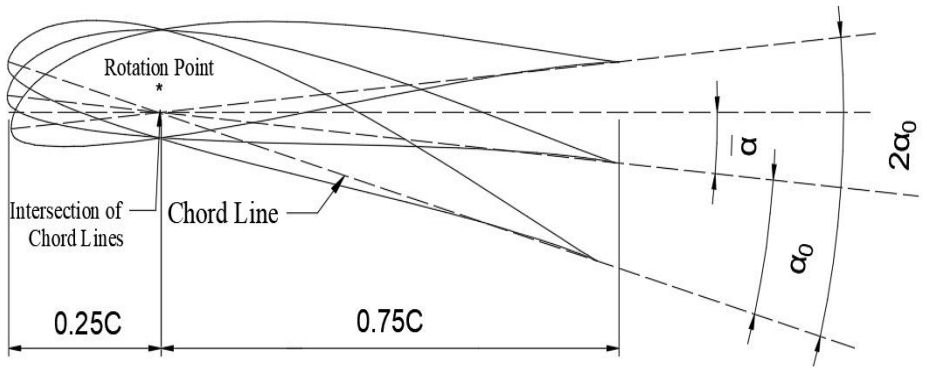

Figure 5 Details of pitch oscillating motion in SD7062 airfoil

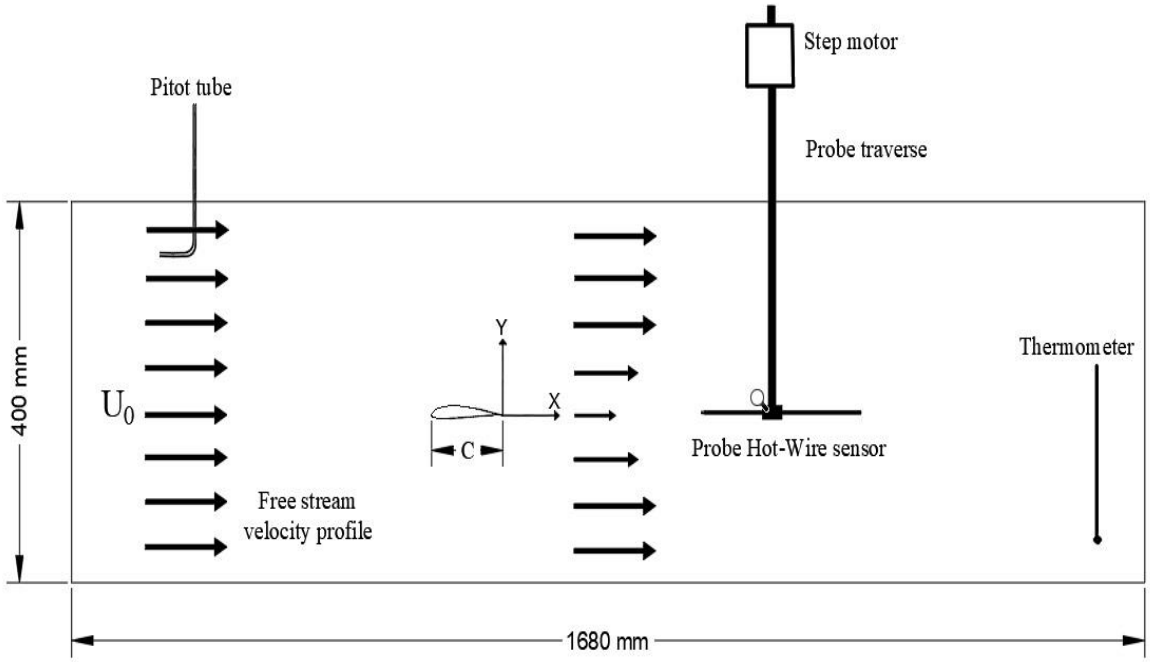

Figure 6 Schematic view of the model in the test section.

Figure (6) presents the schematic view of the model in the test section. The existence of airfoil in the way of free stream flow creates a wake on the back of the model.

The velocity is measured using a hot-wire sensor. The position of the hot-wire sensor is controlled by the traverse mechanism. This mechanism uses three step-motors for each direction. A pitot tube measures the static and total pressure of the free stream flow and obtains the velocity of the free stream by calculating the dynamic pressure. A thermometer senses the temperature of the passing air on the wind tunnel.

Figure (7) shows the block diagram of the wind tunnel test section from Y-Z axis orientation, representing the devices and mechanisms used in this experiment. In the following, each of the mechanisms along with the shape of the devices is explained in some details.

Figure (8) displays the apparatus used in the pitching mechanism. In the pitching mechanism, the motor driver sets the frequency of pitching, and the controller runs the motor driver manually. Servomotor, crankshaft, and universal joint rotate the airfoil by specified frequency. The rotation amplitude is controlled by an off-center connection between the amplitude adjustment disk and the crank system.

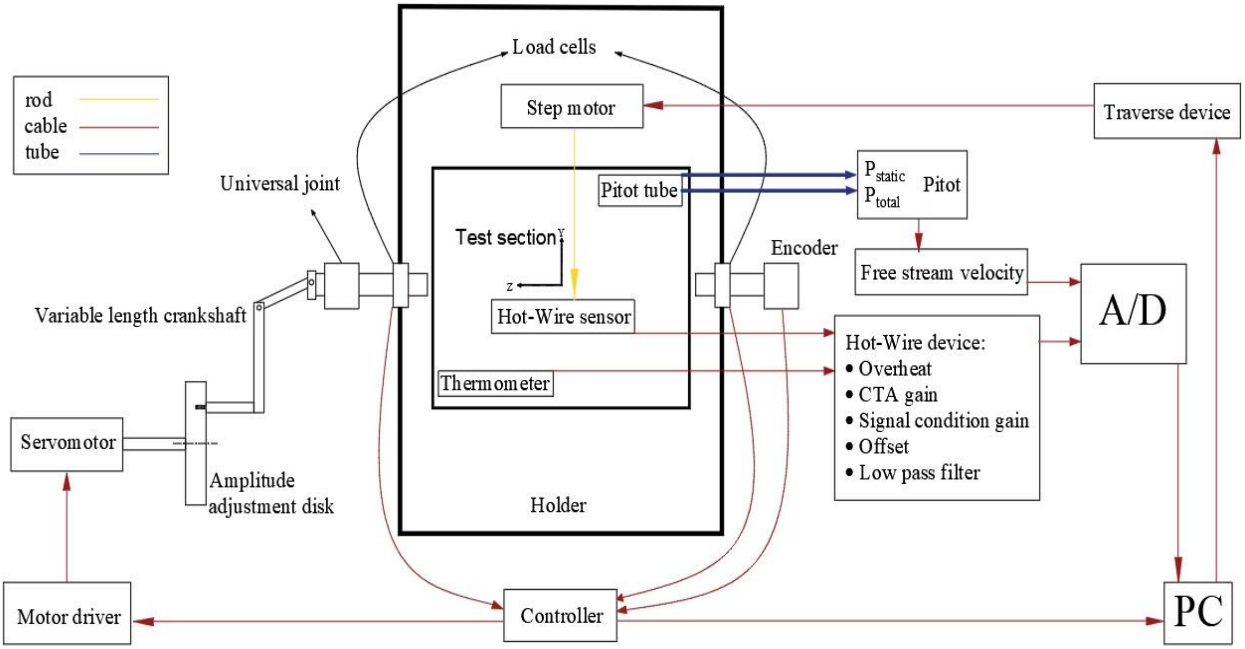

Figure 7 Schematic view of wind tunnel mechanisms and devices

a) Motor driver

b) Controller

c) Servomotor

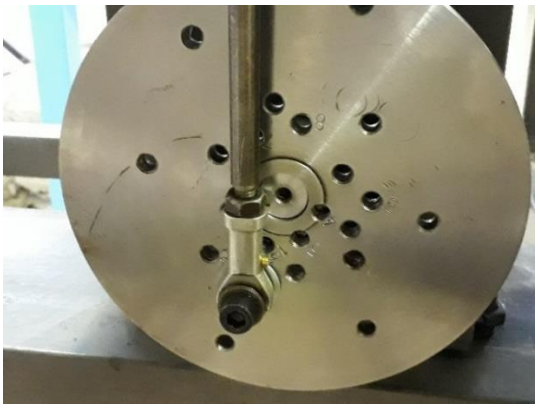

d) Amplitude adjustment disk

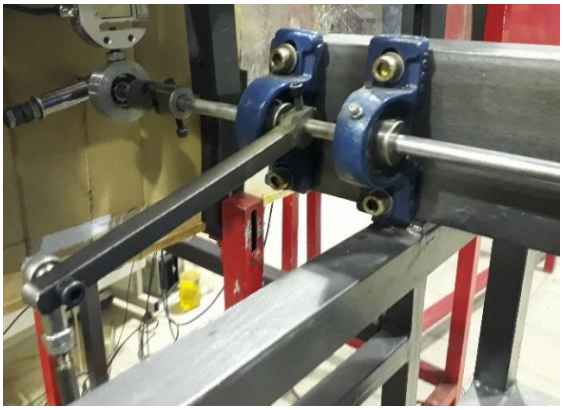

e) Crankshaft

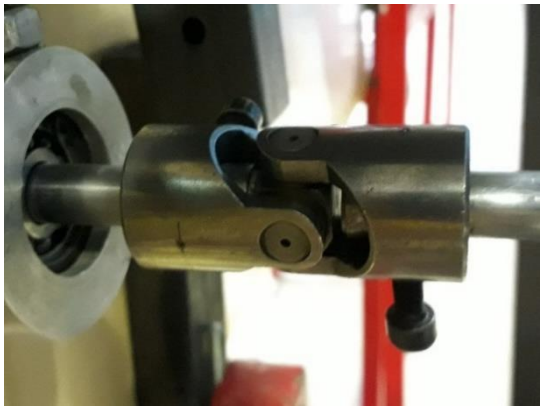

f) Universal joint

Figure 8 Devices used in the oscillating mechanism

a) Traverse device

b) Step-motor

c) Pitot device

d) Hot-wire device

Figure 9 Traverse and hot-wire mechanisms installed in the Laboratory of Aerodynamics at HSU

Figure (9) represents the traverse and hot-wire devices used in our wind tunnel. The traverse device runs the step-motors to guide the hot-wire sensor to the specified position. Pitot tube measures the velocity of free stream flow and gives its data to PC by A/D (Analogue to Digital device). Hot-wire sensor and thermometer transmit the measurements to hot-wire device. This hot-wire device accomplishes the overheating of the sensor, CTA gaining, signal condition gaining, offsetting, and low pass filtering of the collected data and transmits the results to A/D. Finally, A/D converts the analog signals into digital signals and sends these digital signals to the PC. In summary, the forces and velocity profile can be measured over time through the aforementioned mechanisms.

The hot-wire anemometer probe is a one-dimensional SN (Single Normal). Wire of the sensor is made of tungsten with a diameter of 5 micrometers. These sensors are designed to measure fluid flow with high TI. These sensors are created by Fara Sanjesh Saba (FSS) company (see the characteristics in table (2)).

The probe is mounted on a supporting rod in the center of the airfoil span. The wake profiles are measured at seven downstream stations: X/C = 0.28, 0.62, 0.96, 1.31, 1.66, 2, and 2.34. The probe is traversed in a non-dimensional length Y/C ranging from -0.7 to +1. The measurement positions along the Y-axis are taken at 2-mm intervals.

The sampling rate is one of the essential parameters in choosing a DAQ card. Hot-wire anemometer is capable of measuring the instantaneous velocity with a frequency of more than 50 kHz. The sampling rate should follow the Nyquist rule to gather the correct data. According to the Nyquist theorem, the sampling rate should be more than two times the highest frequency required to be recorded. This frequency is specified in the signal adopting circuit using a low-pass filter. The frequency of turbulent flow is determined according to the type of the fluid flow and Reynolds number. This frequency is the highest frequency required, and the sampling rate is determined based on it. In the current study, the frequency of mean sampling, the frequency of instantaneous sampling, time of the sampling, and cut-off frequency are chosen at 5000 Hz, 10000 Hz, 25 s, and 16000 Hz, respectively.

Freestream velocities for measuring the characteristic properties of airfoil are 15 and 25 m/s. The corresponding Reynolds numbers based on the chord length are Re_1=153169 and Re_2=255282, respectively.

Non-dimensional reduced frequencies of k are 0.05, 0.08, and 0.12. Therefore, frequencies of oscillation according to freestream velocities are 1.65, 2.63, and 3.95 Hz for Re_1, and 2.75, 4.4, and 6.6 Hz for Re_2.

The uncertainty in devices and mechanisms to measure the aerodynamic characteristics are listed according to table (3). The table indicates that the total uncertainty in measuring the velocity is below %2.

Table 2 Characteristics of the hot-wire sensor probe used in this experiment

Manufacturer	Model	Type	Characteristics
Fara Sanjesh Saba (FSS)	WP11	Plated Single Normal(SN)	$D_s = 2.9mm$ $L_s = 25mm$ $L_p = 6.5mm$ $S = 3mm$ $S_e = 1.25mm$

Table 3 Considered uncertainty in the tests

Type of uncertainty	Uncertainty value
Uncertainty in velocity measurements using pitot tube and pressure transducer	0.008
Uncertainty in the traverse mechanism	0.003
Uncertainty in the A/D board resolution for 12 bit and 10V	0.0008
Uncertainty in the ambient temperature variations	0.003
Uncertainty in spline curve fitting	0.005
Total	0.0198

3 Validation

The experimental study of reference [41] is used to validate the results of the pitching motion. In this research, NACA0012 airfoil is used under the following conditions: chord length and width of the airfoil are 145mm and 450mm, respectively. The mean AoA is 2.5 degrees, and the amplitude is 8 degrees. The oscillation frequency is 1, 2, and 3 Hz. The tested Reynolds number is 50000. Three cases of oscillation frequencies are examined for assessing the results. Also, the mean velocity profiles are compared and illustrated in figure (10). The results of this research were in accordance with the results conducted by Sadeghi et. al. [41]. The percentage of error is less than %5 in each case. Therefore, the accuracy of the laboratory devices and the measurement method are acceptable and validated.

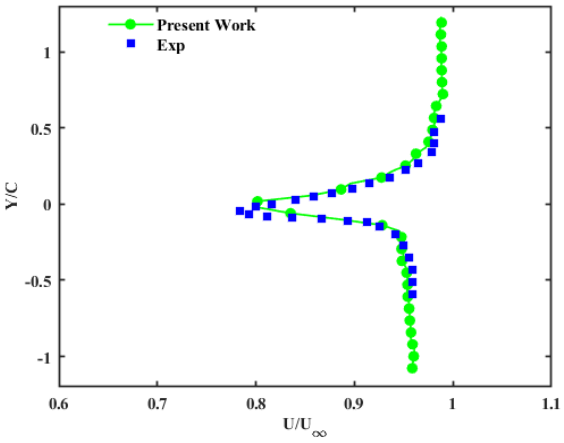

a) Oscillation frequency equals 1 Hz

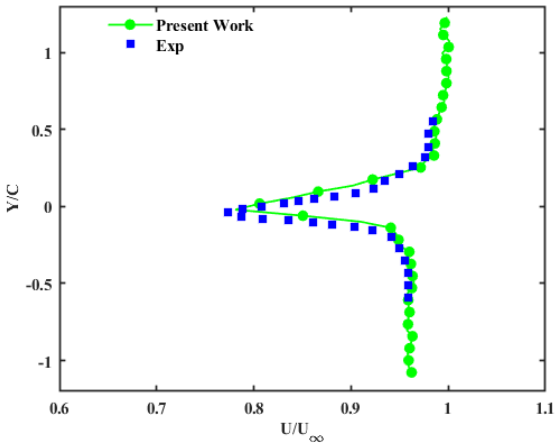

b) Oscillation frequency equals 2 Hz

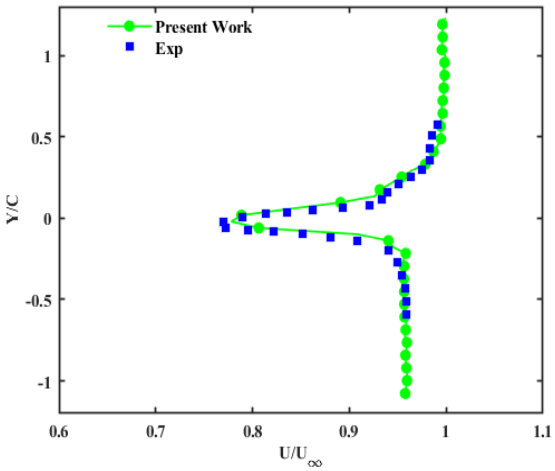

c) Oscillation frequency equals 3 Hz

Figure 10 Comparison of the results of the present study with the reference [41]

4 Governing equations

In this research, the effective parameters on the behavior of the wind turbine airfoil were assessed. Different effective parameters on the airfoil are introduced as follows:
Reduced frequency of oscillation introduced as equation (2):

$$k = \frac{\pi f C}{U_\infty} \tag{2}$$

Where, f is the frequency of oscillations, C is the chord's length and U_∞ is the freestream velocity. The reduced frequency is defined as the flow unsteadiness around the airfoil and blades i.e. a relation between the convective time scale (C/U) and time scale is (1/ω). When the reduced frequency is zero, the flow is in steady state and when $0 < k < 0.005$, the flow is in quasi steady state and when $k > 0.005$, the aerodynamic flow is unsteady [42].
The Reynolds number is calculated based on the chord length and defined as equation (3):

$$\mathrm{Re} = \frac{U_\infty C}{\nu} \tag{3}$$

Where the ν is the kinematic viscosity. The relation of TI and velocity defect are calculated from equation (4) and equation (7) respectively.

$$\%TI = \frac{u_{r.m.s}}{U_\infty} \times 100 = \frac{\sqrt{\overline{u'^2}}}{U_\infty} \times 100 \tag{4}$$

$$u' = U - \overline{U} \tag{5}$$

$$\overline{U}(x,t) = \lim_{T\to\infty} \frac{1}{T} \int_{t_0}^{t_0+T} U(x,t)\,dt \tag{6}$$

$$\frac{W_0}{U_\infty} = \frac{U_\infty - U_{\min}}{U_\infty} \tag{7}$$

Where the u_{rms} is the fluctuation terms of velocity and $U_{\min}$ is the minimum velocity in the wake of the model.

5 Results and discussion

Figure (11) shows a comparison between the mean TI at diverse stations for static airfoil and different AoAs. The results infer that at AoAs under 11 degrees, the farther the data location from the model, the lower the TI due to the attached flow on the airfoil in these AoAs. Thus, no Leading Edge Vortex (LEV) is formed, and the TI profile has one peak in all stations. However, in the first station at AoA of 20 degrees two peaks are observed in the TI profile, where TI is decreased in the center of the wake. The reduction in TI is a consequence of the low-pressure field in the middle of the Trailing-Edge Vortex (TEV) at this AoA. To the contrary, the TI increases dramatically at the boundary of the TEV to free streamflow. It is also observed that the higher the Reynolds number of the flow, the lower the TI and half-width ($b_{1/2}$) caused by higher free stream velocity and momentum in higher Reynolds. Besides, it is found that the more AoAs, the more TI because larger vortices are created. Larger vortices increase the rotation of the flow, which highly mix the fluid layers and TI.
The results show that at the first station and zero AoA, the maximum TI occurs exactly at y/c=0, and at farther stations, it tilts very slightly down the airfoil. Because at zero AoA, the flow is attached to the airfoil, and the flow separation point will be at TE, creating a very small TEV. Due to the different pressure gradients at the top and beneath the airfoil, the flow velocity over the airfoil is higher than the flow velocity under it, so the resulting vortex is formed clockwise(CW). Due to its rotation, this vortex is inclined downwards in farther stations.
The maximum TI occurs below the airfoil at AoA of 11 degrees and first station. According to the downwash direction, the maximum TI goes downward in farther stations due to the CW vortex at the TE. These effects are the opposite for AoA of -11 degrees. For instance, in the

AoA of -11 degrees, the maximum point of turbulence will be above the y/c=0 due to the counter-clockwise(CCW) vortex.
The flow is stalled at AoA of 15 degrees. Therefore, at AoA of 20, the separation occurs near the LE. Two vortices are created in the wake of the airfoil, one CW over the airfoil and the other CCW under the airfoil. Because at AoA of 20 the reverse pressure gradient is very high, the separation point of the flow on the airfoil moves to LE, and a large CW vortex is created on the airfoil. A CCW vortex is created at TE because the pressure is high under the airfoil and low over it. The effect of these two vortices on the farther stations is gradually diminished. Unfortunately, in this experiment, due to the limited length of the wind tunnel test section, we could not achieve the state that the effects of these two vortices are completely eliminated, but it can be seen that at x/c=2, the effects of vortices are reduced also, Reynolds number greatly reduces the effects of vortices.

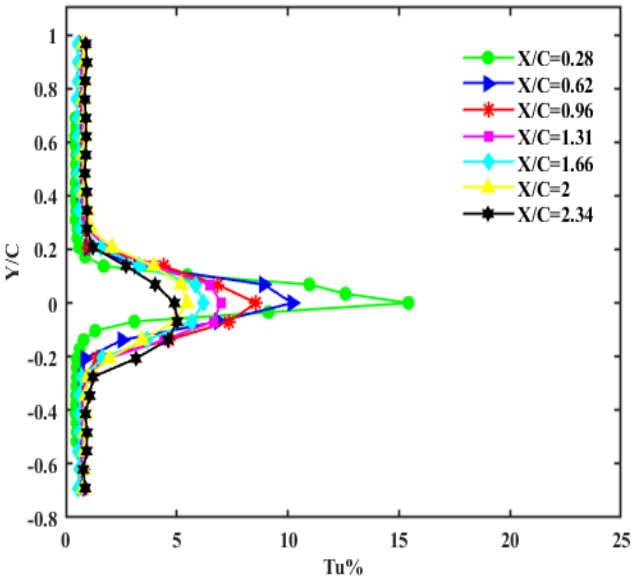

a) AoA: Zero, Re_1

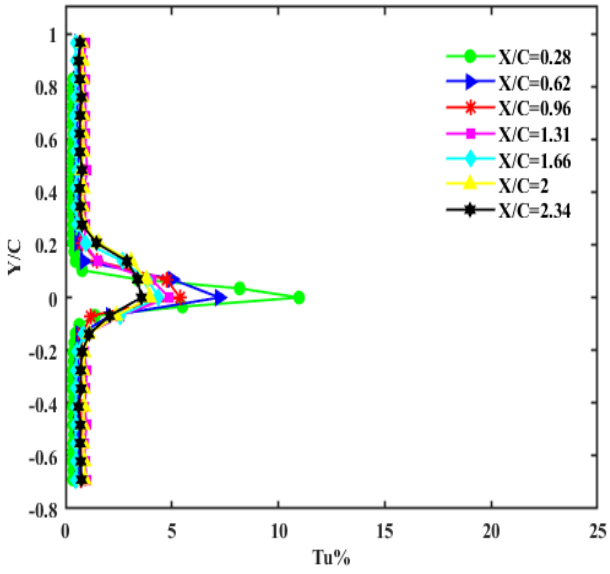

b) AoA: Zero, Re_2

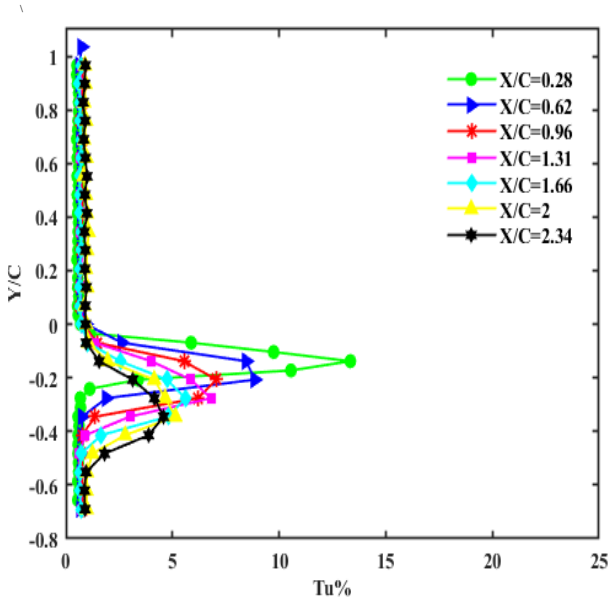

c) AoA: 11°, Re_1

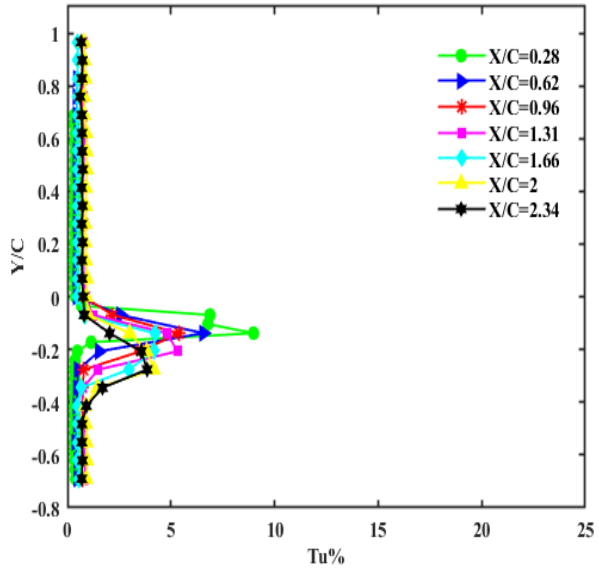

d) AoA:11°, Re_2

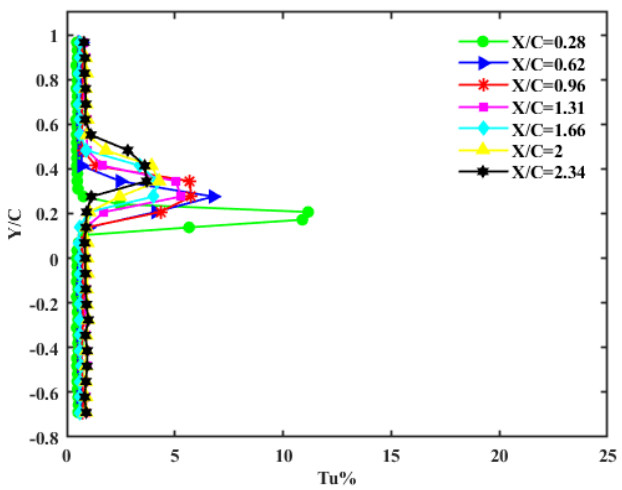

e) AoA:-11°, Re_1

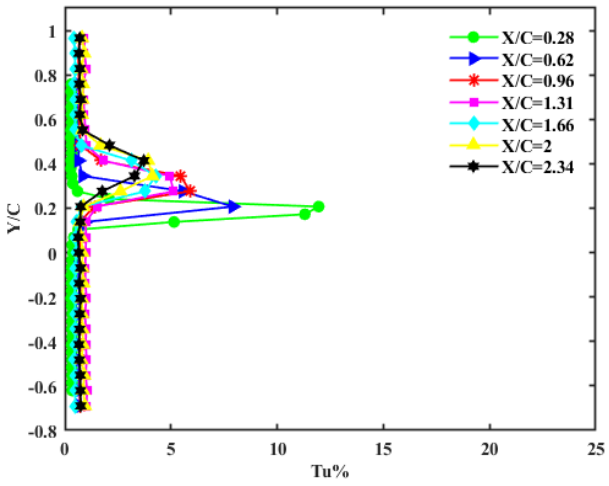

f) AoA:-11°, Re_2

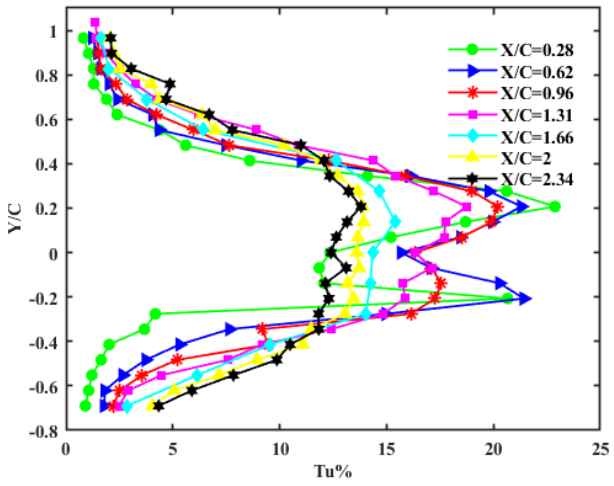

g) AoA:20°, Re_1

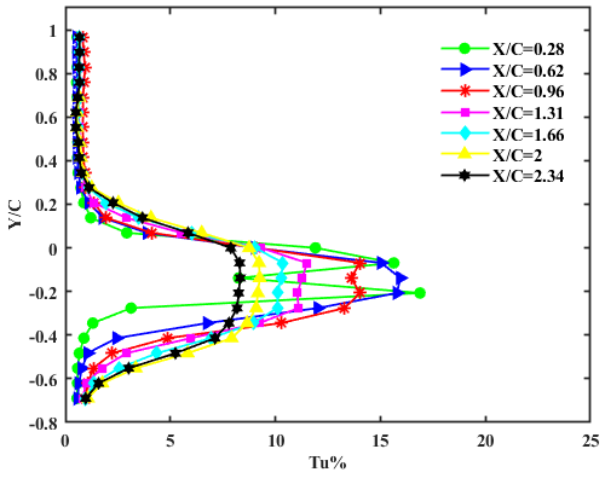

h) AoA:20°, Re_2

Figure 11 Comparison of mean TI for different AoAs (static airfoil).

Figure (12) shows a comparison of mean TI for two different reduced frequencies, 0.05, and 0.08, at different stations for symmetry (amplitude varied from 11 to -11 degrees) (See figure (12a) to figure (12d)), and 0.05 reduced frequency in asymmetry oscillation (amplitude varied from 0 to 20 degrees) (See figure (12e) and figure (12f)). Figure (12) presents that the reduced frequency is positively correlated with TI in symmetry and asymmetry oscillation. For both cases, TI value shrinks and gets wider in stations farther away from the airfoil. Similar to the static airfoil, Reynolds number is inversely proportional to TI value, which means by increasing Reynolds number, we should expect a lessening in TI value. For symmetry oscillation, two peaks are observed within the TI profile. One CW at AoA of 11 degrees and the other CCW at AoA of -11 degrees. Because figure (12) shows the average values of TI in the oscillating airfoil, the effect of both vortices is observed. The shape and the strength of these two vortices are non-identical as the airfoil is asymmetrical.

There is only one peak for asymmetry oscillation, which means only one vortex is formed in the wake because the effect of high AoAs is dominant to the airfoil shape. Also, in this case, the TI was much higher than the symmetric oscillation because of forming as large-scale vortices are formed in asymmetric motion, unlike the symmetrical one. We should focus on the instantaneous TI data for recognizing the exact size of the wake vortices, which comes as follows.

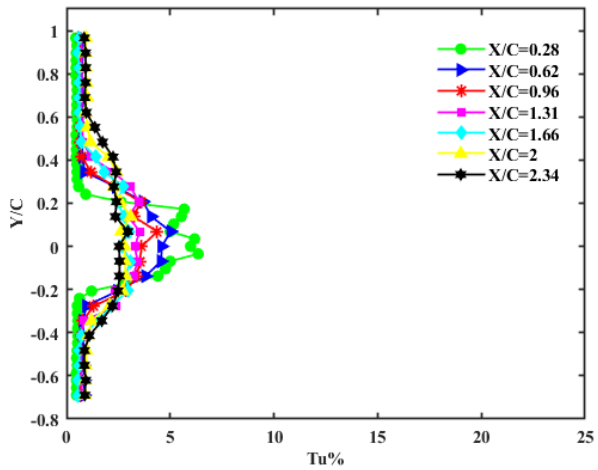

a) symmetry oscillation, k=0.05, Re_1

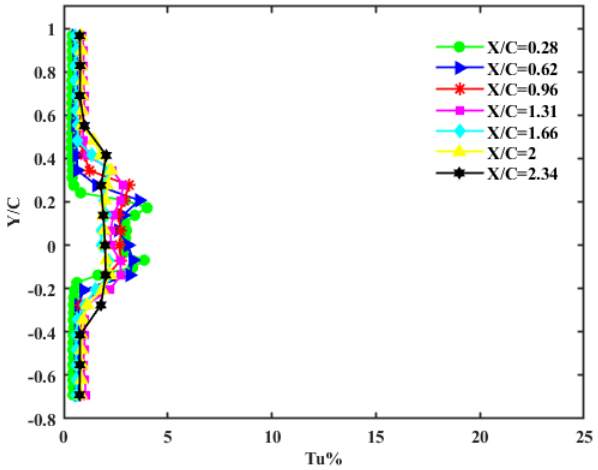

b) symmetry oscillation, k=0.05, Re_2

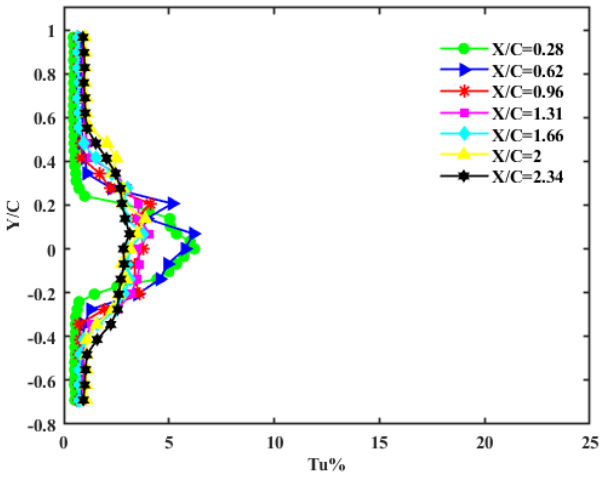

c) symmetry oscillation, k=0.08, Re_1

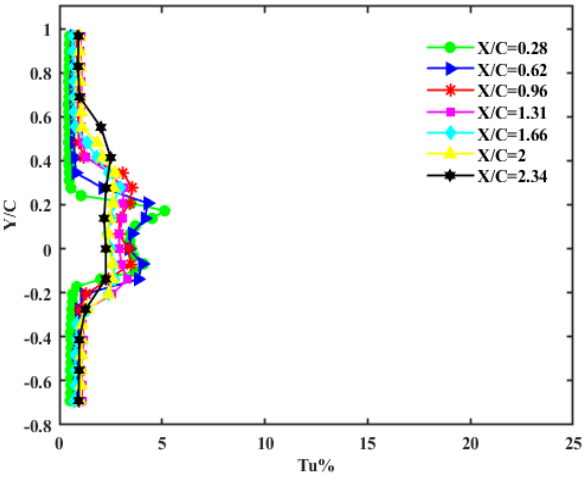

d) symmetry oscillation, k=0.08, Re_2

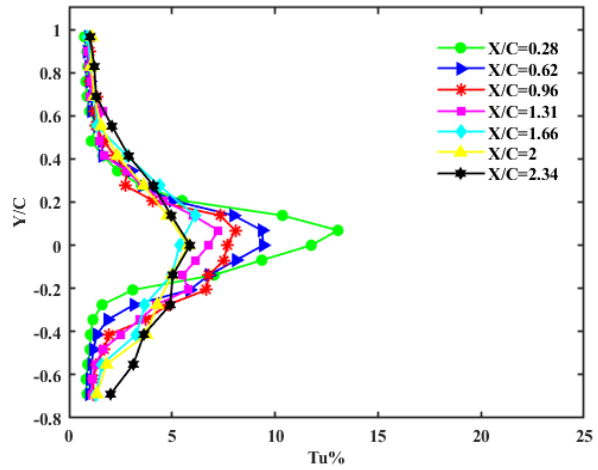

g) asymmetry oscillation, k=0.05, Re_1

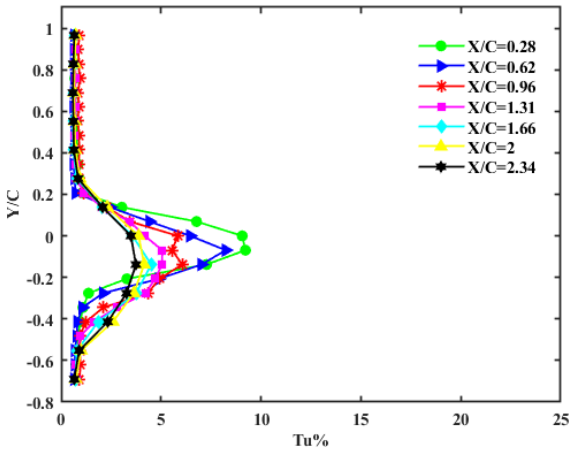

h) asymmetry oscillation, k=0.05, Re_2

Figure 12 Comparison of mean TI for different reduced frequencies (symmetry and asymmetry oscillation)

Figure (13) represents a comparison between the instantaneous TI values at different states. The measured instantaneous equals mean TI for static airfoil (See figure (13a)). Statistical data

provides mean measurement properties of passing flow over the airfoil. Thus, statistical data could be considered for calculating the upcoming force on the airfoil in the static airfoil. There is a different scenario in oscillating motion because the measured instantaneous TI value is far from the measured mean TI. In symmetry oscillation at X/C=0.28 and Re1 for instance, although maximum measured TI in the instantaneous state is %40, the maximum measured TI from statistical data is around %15 (See figure (13b)). Regarding the oscillating case, two vortices are formed in the wake; One of these vortices is CW for positive AoAs, and the other is CCW for negative AoAs. These vortices impact dynamic forces into the airfoil. Accordingly, dynamic forces are to be considered as well as static forces using instantaneous data. In other words, it is essential to consider both statistical and instantaneous data for calculating the forces acting on the airfoil while choosing the appropriate material for the production of dynamic airfoils. Figure (13c) shows that as the Reynolds number increases, the TI decreases. The reason for this is that as the free-flow velocity increases, the velocity fluctuations also increase, but this increase in fluctuation velocity components is not proportional to the increase in free-flow velocity, so the ratio of root mean square of fluctuation velocity to free-flow velocity, which represents TI, will be smaller.

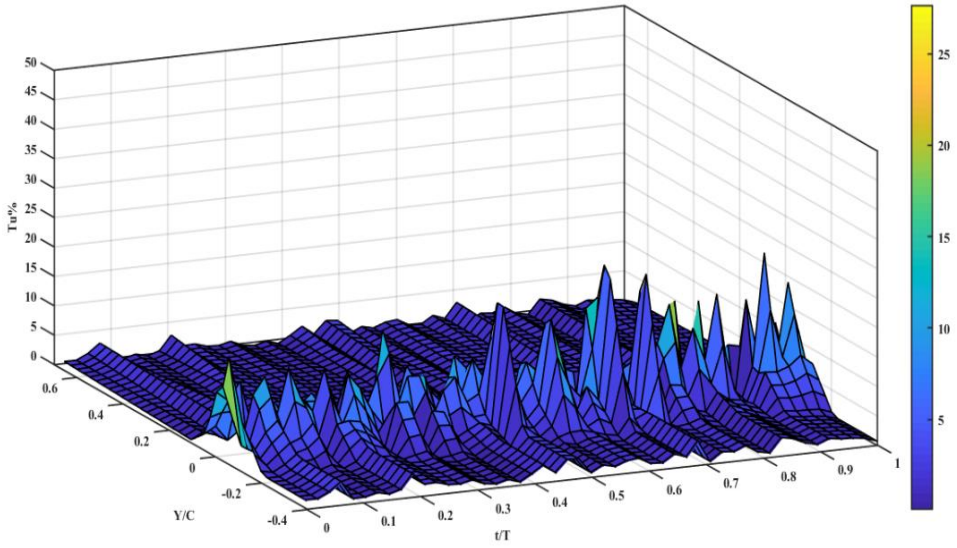

a) instantaneous TI for the static airfoil, AoA: zero, X/C=0.28, Re_1.

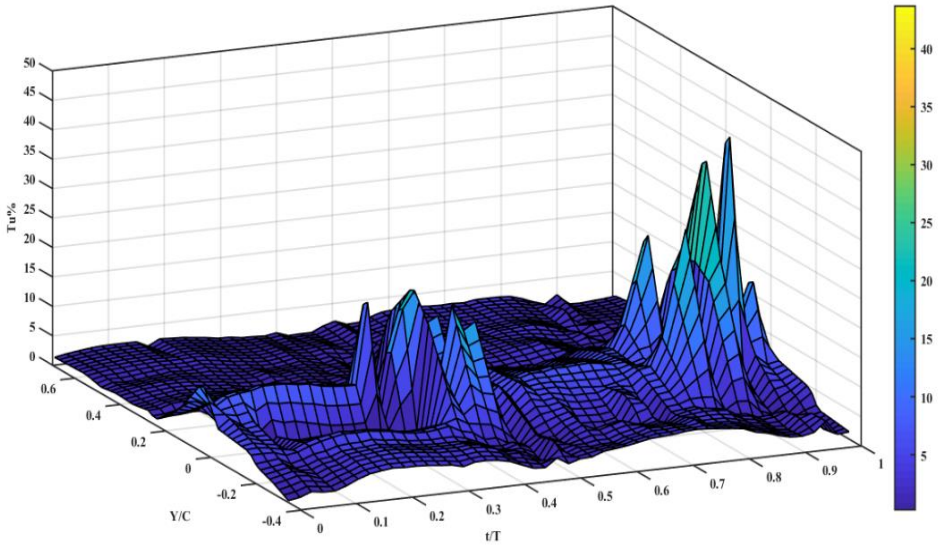

b) instantaneous TI for symmetric airfoil, k=0.05, X/C=0.28, Re_1.

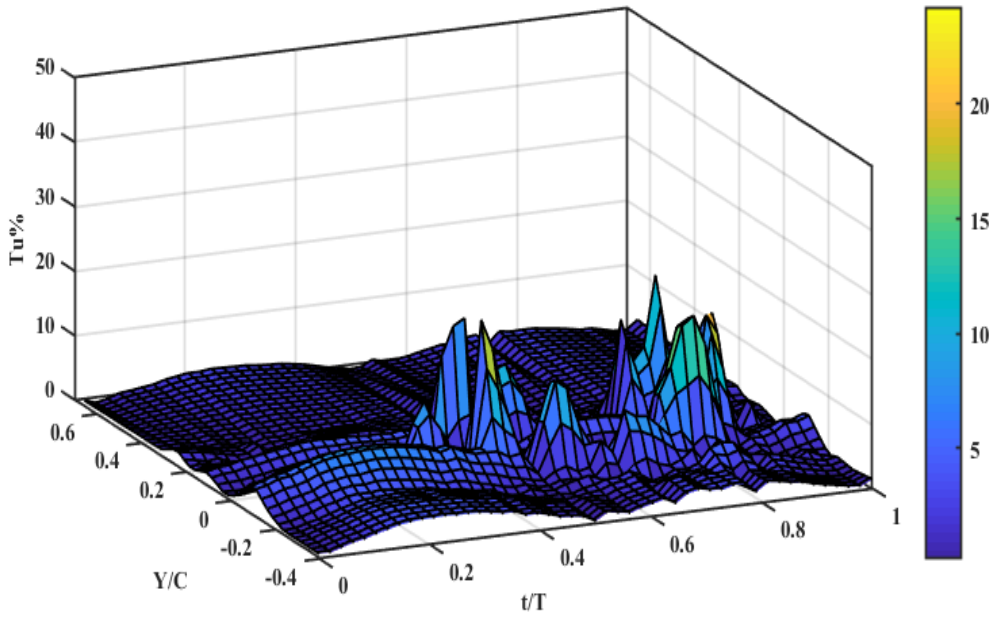

c) instantaneous TI for symmetric airfoil, k=0.05, X/C=0.28, Re_2.

Figure 13 Comparison of instantaneous TI for different states

Figure (14) represents a comparison of mean velocity for Re_1 and Re_2 at different AoAs in the case of the static airfoil. The maximum velocity defect is inversely correlated to AoA, because with increasing the AoA, the pressure difference between the front and back of the airfoil increases, and as a result, a larger wake is formed, and this larger wake will cause a greater velocity defect. Figure (14a) and (14b) depict that the maximum velocity defect occurs right behind the model whereas figure (14c) and (14d) show that at AoA of 11 degrees, the highest velocity defect occurs at the bottom of the airfoil. Figure (14e) and (14f) show that at AoA of -11 degrees, the highest velocity defect happens at the top of the airfoil. Figure (14g) and (14h) present that at AoA of 20 degrees, the highest velocity defect occurs near the bottom of the airfoil. The wake thickness at AoA of 20 degrees is much higher than AoAs of zero, 11, and -11 degrees. Higher Reynolds Number leads to the narrower wake thickness since the momentum force is dominant (rather than the viscous force) at high Reynolds numbers. In all static airfoil cases, only one peak at the mean velocity profile can be observed, demonstrating that only one vortex has been formed in the wake at the trailing edge. It is noteworthy mentioning that advancing the Reynolds number leads to a stronger vortex.

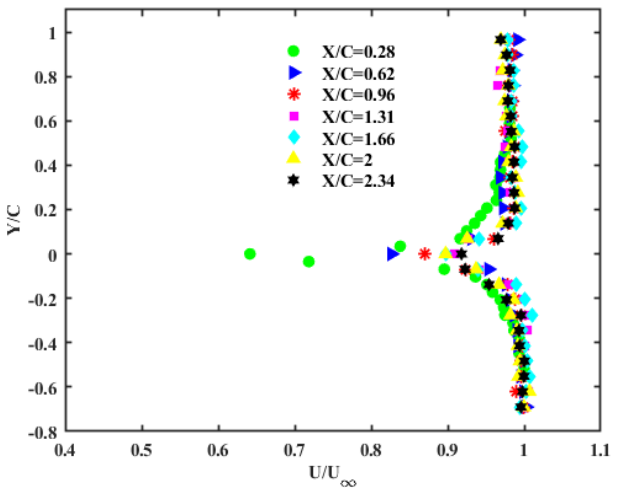

a) AoA: Zero, Re_1

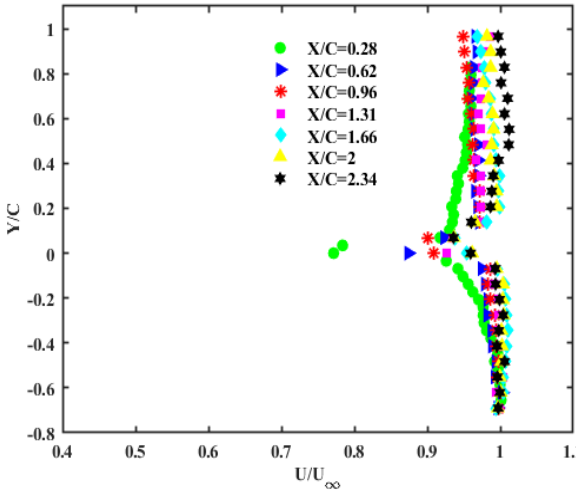

b) AoA: Zero, Re_2

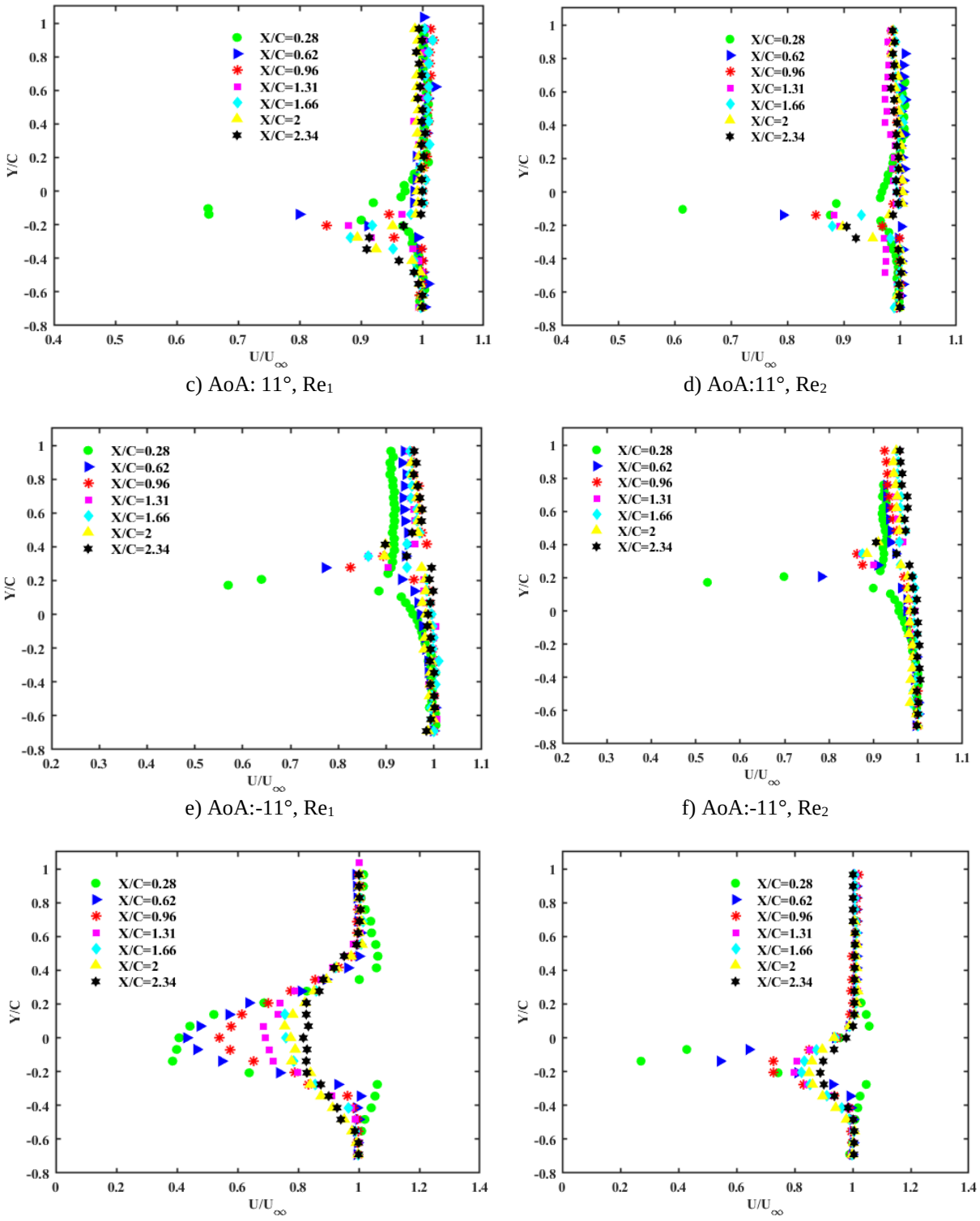

c) AoA: 11°, Re_1 d) AoA:11°, Re_2

e) AoA:-11°, Re_1 f) AoA:-11°, Re_2

g) d) AoA:20°, Re_1 h) d) AoA:20°, Re_2

Figure 14 Comparison of mean velocity for different AoAs (static airfoil)

Figure (15) shows a contrast of mean velocity for different reduced frequencies and Reynolds numbers in the case of symmetry and asymmetry oscillation. The velocity defect gets smaller far away from the model while the wake amplitude becomes width. The reason for this phenomenon is dominating the viscous forces to momentum forces at far away stations. The kinetic energy cascades down from large to small eddies by interactional forces between the eddies. At a microscopic scale, the energy of the vortices dissipates into heat due to viscous forces. Figure (15a) to figure (15d) show the mean velocity profile for different reduced

frequencies and denoted two peaks in these profiles. Two vortices are formed in the wake of symmetry oscillation. However, the shape and strength of these two vortices are non-identical as the airfoil is asymmetrical. Contrary to the symmetry oscillation, only one vortex is formed in the wake of asymmetry oscillation. But the size of the vortex in asymmetry oscillation is much larger than the size of two vortices in symmetry oscillation because the pressure gradient is much higher in case asymmetric oscillation. The amplitude of the wake in pitching motion is considerably wider than the static state. The reason is that in an oscillating motion, pitching airfoil helps the flow diffuse into the potential flow faster and broader than stationary airfoil. In other words, a pitching airfoil denies forming a strong vortex compared to a stationary airfoil at the same AoA. That's why no stalls are observed in the oscillating airfoil at AoAs that stall occurs in the stationary airfoil.

Figure (16) compares instantaneous stream velocity in different states. The measured instantaneous velocity is the same as the measured mean velocity for the stationary airfoil. Thus, the statistical data provides average measurement properties of passing flow over the airfoil that can be taken into account to calculate the upcoming forces on the airfoil. However, these data fail to describe the oscillatory motion, as the measured instantaneous velocity differs from the measured mean velocity for pitching airfoil. For example, in symmetry oscillation at X/C=0.28 and Re_1, the measured velocity defect in the instantaneous state is about 0.5, but the measured velocity defect from statistical data is around 0.15. Two peaks are observed in the wake of oscillating motion, which means two vortices are formed in this case, developing tremendous dynamic forces on the airfoil. Therefore, for the process of designing the oscillating airfoil, considering only statistical forces would be entirely inadequate. In order to present a suitable designing, it seems crucial to study both statistical and instantaneous data to calculate the forces acting on the airfoil while selecting the appropriate material for the production of the airfoil.

Figure (17) represents an illustrating comparison of maximum velocity defects under different states. Figure (17a) and (17b) show that the velocity defect for the zero AoA is the lowest, and the AoA is proportional to the velocity defect. The velocity defect points are adjacent in AoAs of 11 and -11 degrees, and the difference of this velocity defect can result from the asymmetry of the upper and lower side of the airfoil. The velocity defect at the AoA of 20 degrees is heterogeneously higher than the others due to stall conditions. The velocity defect at the following stations does not follow a regular trend for the Re_1. According to previous experiments [43], the SD7062 airfoil stalls at a AoA of 15 degrees. The wake of this airfoil develops entirely asymmetric and heterogeneous after stalling. Therefore, the velocity defect parameter after stall is heterogeneous. This velocity defect is increased in asymmetry motion compared to the symmetry motion. Also, the Reynolds number rarely affects the maximum velocity defect in oscillating motions.

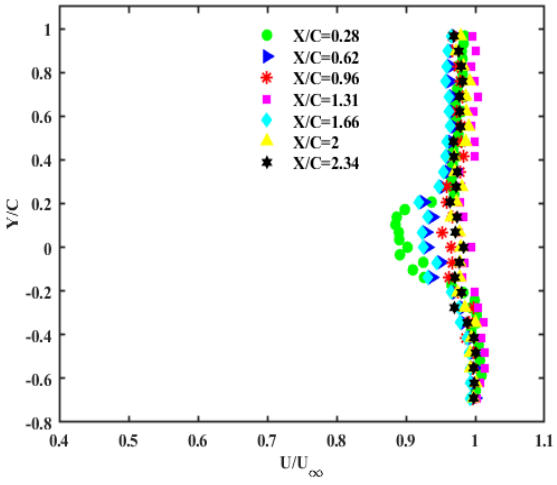

a) symmetry oscillation, k=0.05, Re_1

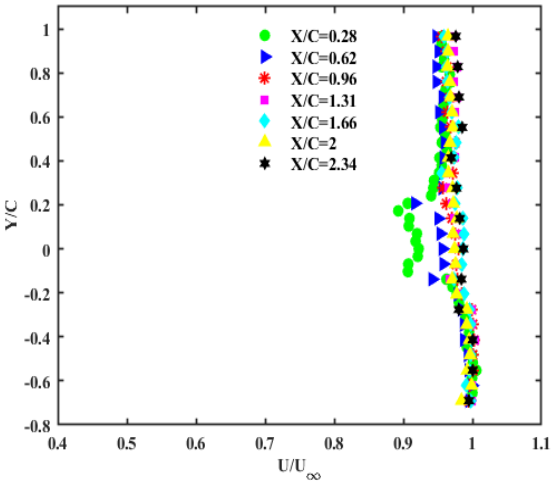

b) symmetry oscillation, k=0.05, Re_2

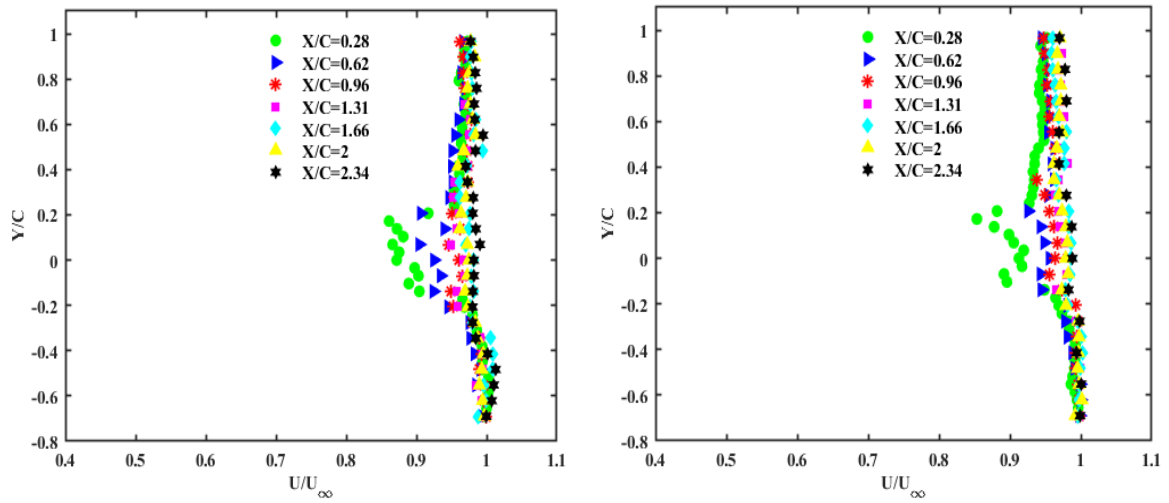

c) symmetry oscillation, k=0.08, Re_1 d) symmetry oscillation, k=0.08, Re_2

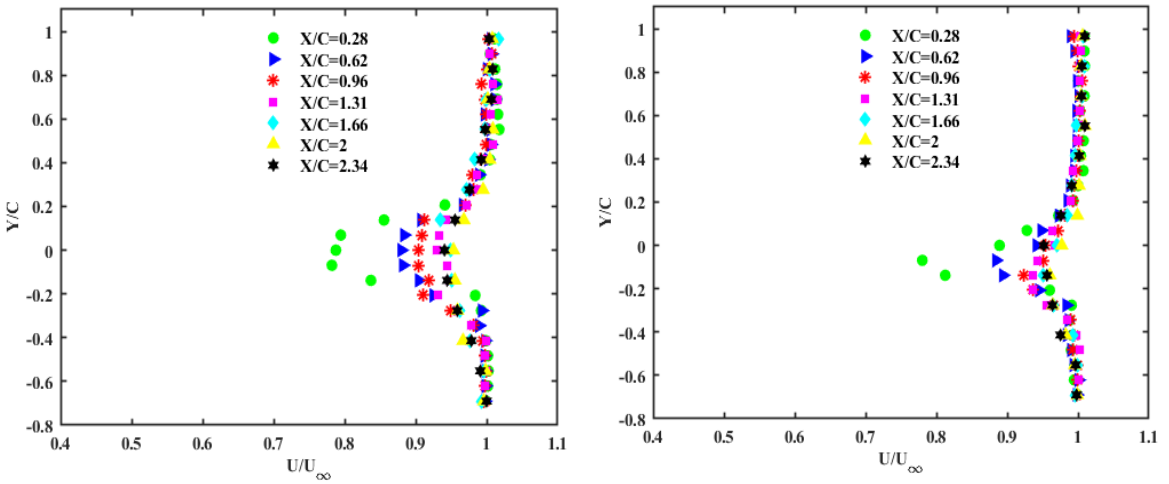

g) asymmetry oscillation, k=0.05, Re_1 h) asymmetry oscillation, k=0.05, Re_2

Figure 15 Comparison of mean velocity for different reduced frequencies (symmetry and asymmetry oscillation)

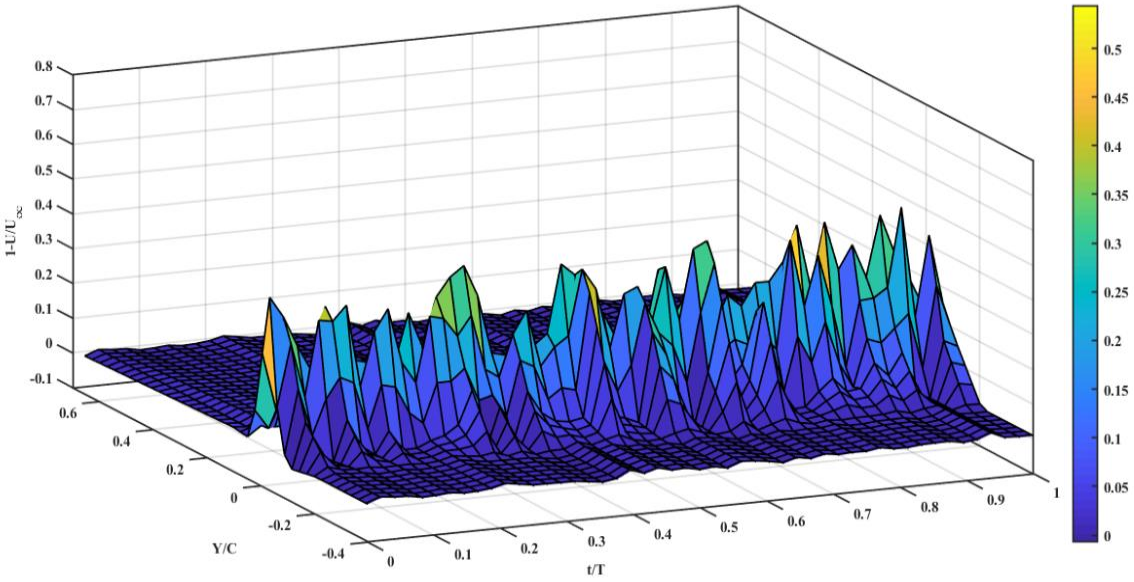

a) instantaneous velocity for static airfoil, AoA: zero, X/C=0.28, Re_1.

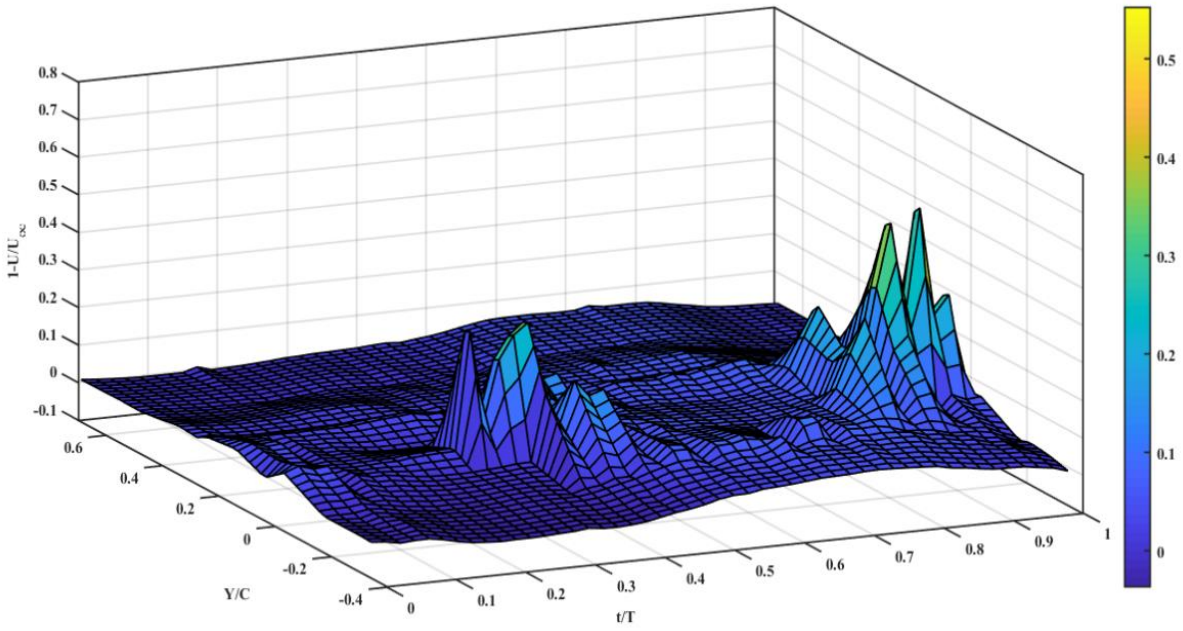

b) instantaneous velocity for symmetric airfoil, k=0.05, X/C=0.28, Re_1.

Figure 16 Comparison of instantaneous velocity for different states

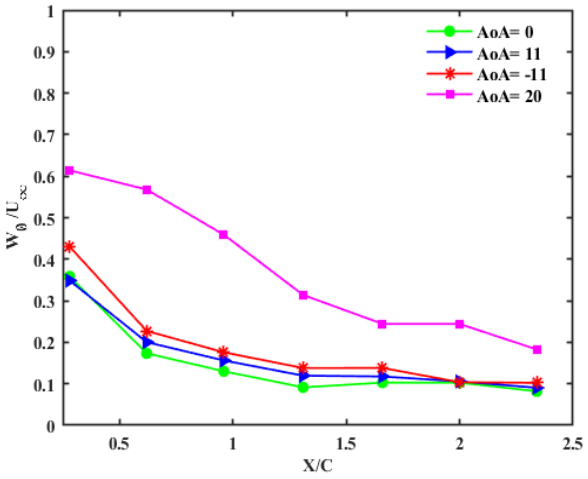

a) static airfoil, Re_1

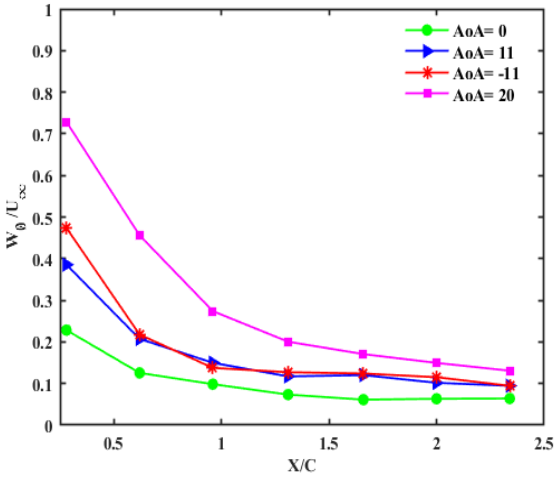

b) static airfoil, Re_2

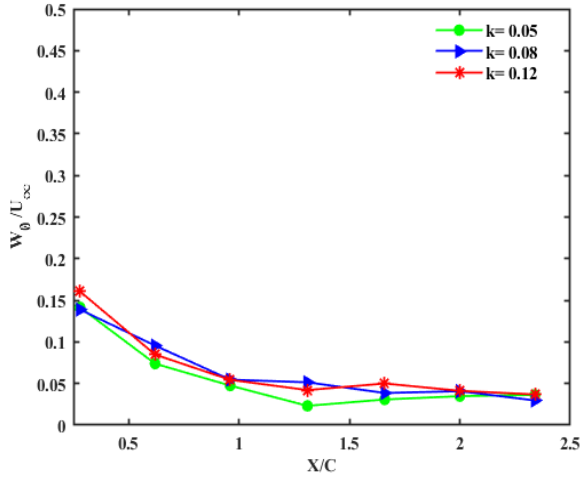

c) symmetry oscillation, k=0.05, Re_1

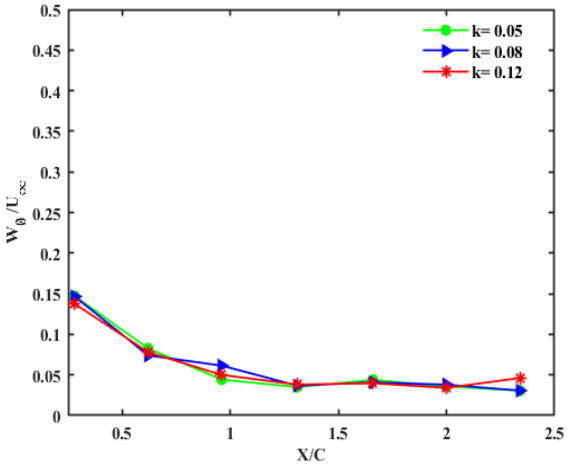

d) symmetry oscillation, k=0.05, Re_2

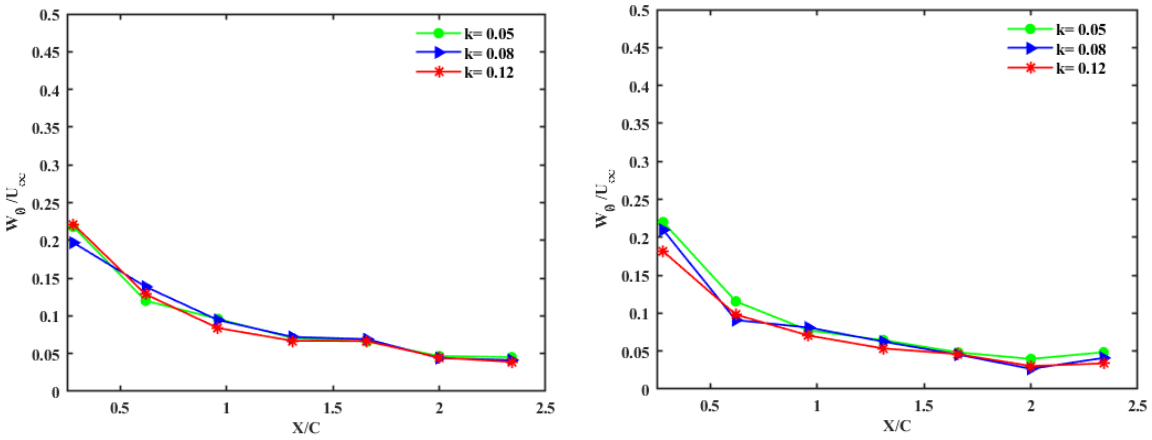

e) asymmetry oscillation, k=0.05, Re_1 f) asymmetry oscillation, k=0.05, Re_2

Figure 17 Comparison of maximum velocity defect for different states.

Figure (18) depicts the relation between maximum TI in different states. Figure (18a) and (18b) show the maximum TI behind the airfoil. By increasing distance from the model, TI falls down in all cases. Also, with increasing AoA, the maximum TI increases. The maximum TI at AoA of 20 degrees is significantly higher than other AoAs, due to the stall conditions at this AoA. In other words, under stall conditions, TI undertakes a significant sudden rise. The Reynolds number rarely affects the maximum TI in pitching motions, but maximum TI lessens as the Reynolds number increases in the stationary airfoil. Asymmetry motion is associated with more maximum TI compared to symmetry motion which is a result of the larger vortex made in asymmetry oscillation.

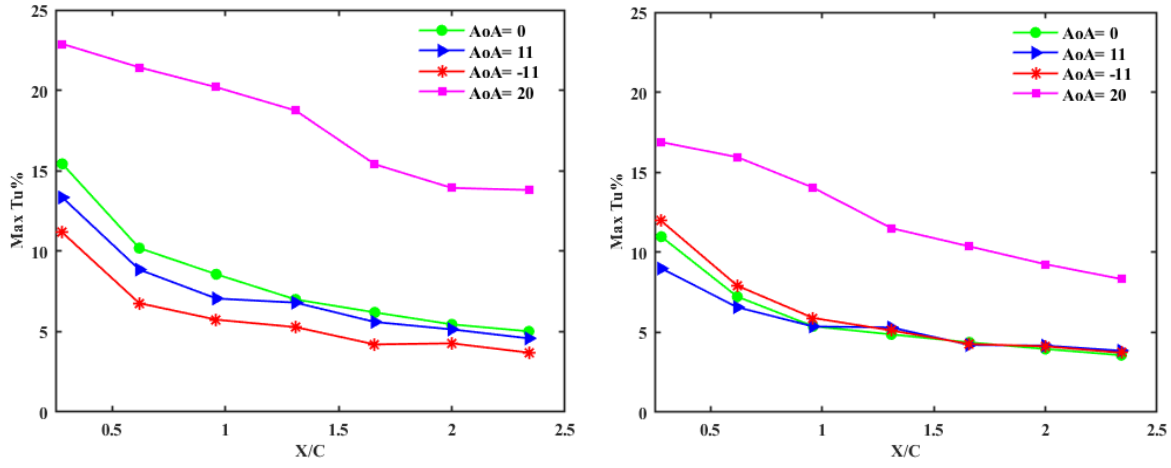

a) static airfoil, Re_1 b) static airfoil, Re_2

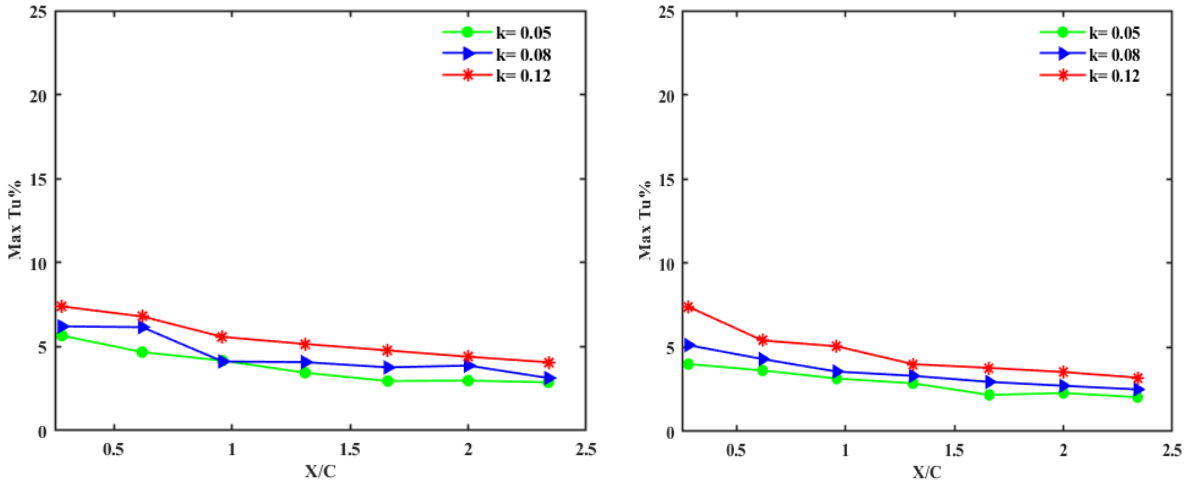

c) symmetry oscillation, Re_1 d) symmetry oscillation, Re_2

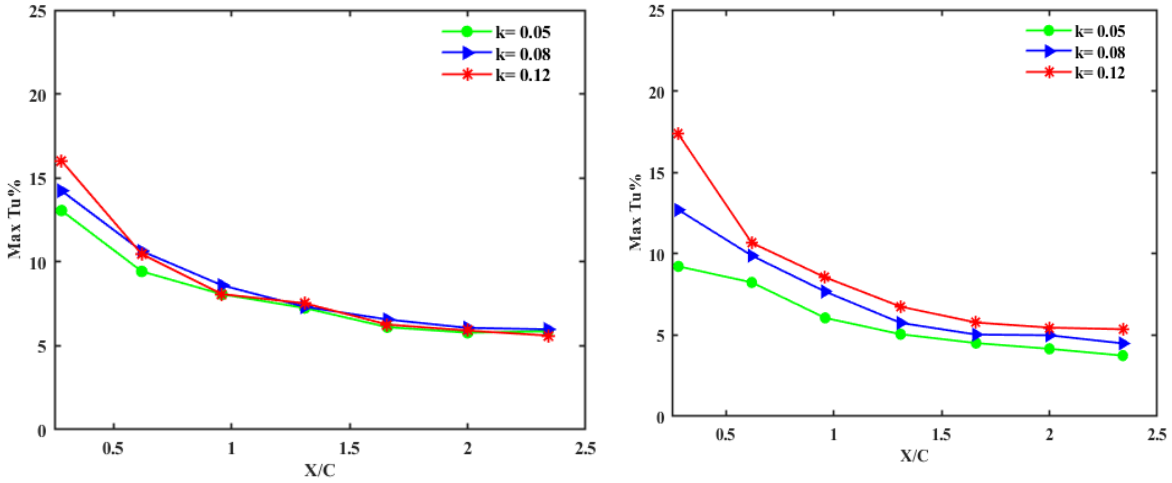

e) asymmetry oscillation, Re_1 f) asymmetry oscillation, Re_2

Figure 18 Comparison of maximum TI for different states

6 Conclusion

In this research, an experimental study was carried out on the effects of several aerodynamic parameters in steady-state and pitching motion of SD7062 airfoil. Concerning the steady-state, the effect of AoAs, Reynolds number, and X/C stations were investigated. Regarding pitching motion, the effect of reduced frequency, Reynolds number, symmetry, and asymmetry oscillation on different aerodynamic properties like velocity and TI were studied as well. These experimental analyses showed that:

For steady-state: TI usually increases and becomes wider while increasing the AoA. TI is inversely proportional to Reynolds number which is as a result of the higher freestream velocity in higher Reynolds numbers, making the TI smaller than low Reynold numbers. The measured instantaneous TI and velocity almost equals their mean values; denoting that in the statistical data, providing average aerodynamic properties of passing flow over the airfoil suffices for calculating the upcoming forced. The maximum velocity defect is inversely correlated to AoA. In AoA of zero, the maximum velocity defect occurs at the back of the model as there is no separation in the suction and the pressure side of the model; Nevertheless, in positive AoAs and negative AoAs the maximum velocity defect occurs at the bottom and the top of the model respectively. All static motion figures present that there is a static stall in AoA of 20 degrees. Moreover, stall creates a stronger vortex causing an increase in velocity defect. The velocity defect is heterogeneously higher among all under stall conditions. Only one peak could be observed at the mean velocity profile, implying that only one vortex is formed in the wake at the trailing edge, where the intensity of the turbulence is decreased in the center of the wake. Also, the vortex size is positively correlated with the Reynolds number, representing the fact that higher Reynolds numbers can cause stronger vortices.

For pitch oscillation state: TI shrinks in farther stations similar to steady-state, but the range of penetration of the TI in the vertical direction becomes wider. Because the kinetic energy cascades down from large to small vortices by interactional forces between the vortices, at a microscopic scale, the energy of the vortices dissipates into heat due to viscous forces. Consequently, the momentum decreases, and the wake becomes wider. Figures of TI grow with increasing the reduced frequency because higher frequency motions develop stronger wakes, while TI is decreased by increasing the Reynolds number. TI in asymmetry oscillation exceed the symmetric one due to the formation of larger vortices in asymmetry motion. Two peaks could be found in the mean TI profile for symmetry oscillation, whereas there is only a peak

for asymmetry oscillation. Generally, in symmetry oscillation, two TEVs appear in the wake. The shape and the strength of these two vortices are non-identical as the airfoil is asymmetrical. However, in asymmetry oscillation, one vortex is formed in the wake because the effect of high AoAs is dominant to the airfoil shape. Thus, the strength of the vortices is related to the airfoil shape, amplitude of the oscillation, and Reynolds number. The Reynolds number rarely affects the maximum velocity defect and maximum TI in pitching motions. Also, the measured instantaneous TI and velocity are quite deviate substantially from their mean values. Hence, considering both mean and instantaneous forces are required for calculating the aerodynamic forces under this condition. However, the dominant variable is instantaneous forces as in some moments, the forces acting on the pitching airfoil reach several times its average state. These results derived from pitch oscillation state indicate that as the impulse forces are the dominant power acting on the airfoil surfaces, dynamic analysis is necessary to calculate the required strength, which enables us to select the suitable materials for the pitch oscillating airfoils.

Conflict of Interest: The authors declare that they have no known competing financial interests or personal relationships that could have appeared to influence the work reported in this paper.

References

[1] Fole, F., "From da Vinci to the Present- A Review of Airscrew Theory for Helicopters, Propellers, Windmills, and Engines", 9th Fluid and Plasma Dynamics Conference, July 14-16, San Diego, USA, (1976).

[2] Reader, K.R., and Wilkerson, J.B., "Circulation Control Applied to a High Speed Helicopter Rotor", 32th Auunal National Forum of the American Helicopter Society, Washington D.C., USA, (1976).

[3] Wilkerson, J.B., Reader, K.R., and Linck, D.W., "The Application of Circulation Control Aerodynamics to a Helicopter Rotor Model", Journal of the American Helicopter Society, Vol. 19, pp. 2-16, (1974).

[4] Keenan, D.P., "Marine Propellers in Unsteady Flow", Ph.D. Thesis, Department of Ocean Engineering, Massachusetts Institute of Technology, Massachusetts, (1989).

[5] Kerwin, J.E., and Lee, C.S., "Prediction of Steady and Unsteady Marine Propeller Performance by Numerical Lifting-surface Theory", Society of Naval Architects and Marine Engineers, Vol. 8, pp. 1-30, (1979).

[6] Gnesin, V., Rządkowski, R., and Kolodyazhnaya, L., "A Coupled Fluid-structure Analysis for 3D Flutter in Turbomachines", ASME Turbo Expo 2000: Power for Land, Sea, and Air, May 8-11, Munich, Germany, (2000).

[7] Srivastava, R., Bakhle, M., and Keith Jr, T., "Numerical Simulation of Aerodynamic Damping for Flutter Analysis of Turbomachinery Blade Rows", Journal of Propulsion and Power, Vol. 19, pp. 260-267, (2003).

[8] Garrick, I., "Aeroelasticity-frontiers and Beyond", Journal of Aircraft, Vol. 13, pp. 641-657, (1976).

[9] Mi, B., and Zhan, H., "Review of Numerical Simulations on Aircraft Dynamic Stability

Derivatives", Archives of Computational Methods in Engineering, Vol. 27, pp. 1515-1544, (2019).

[10] Wu, Q., Huang, B., Wang, G., and Gao, Y., "Experimental and Numerical Investigation of Hydroelastic Response of a Flexible Hydrofoil in Cavitating Flow", International Journal of Multiphase Flow, Vol. 74, pp. 19-33, (2015).

[11] Gharali, K., and Johnson, D.A., "Effects of Nonuniform Incident Velocity on a Dynamic Wind Turbine Airfoil", Wind Energy, Vol. 18, pp. 237-251, (2015).

[12] Shi, Z.W., and Ming, X., "Effects of Unsteady Freestream on Aerodynamic Characteristics of a Pitching Delta Wing", Journal of Aircraft, Vol. 45, pp. 2182-2185, (2008).

[13] Thielicke, W., "The Flapping Flight of Birds: Analysis and Application", Ph.D. Thesis, Department of Ocean Ecosystems, University of Groningen, Groningen, (2014).

[14] Walker, G.T., "The Flapping Flight of Birds", The Journal of the Royal Aeronautical Society, Vol. 29, pp. 590-594, (1925).

[15] Floryan, D., Van Buren, T., and Smits, A.J., "Efficient Cruising for Swimming and Flying Animals is Dictated by Fluid Drag", Proceedings of the National Academy of Sciences, Vol. 115, pp. 8116-8128, (2018).

[16] Hau, E., "*The Wind Resource. In: Wind Turbines*", Springer, Heidelberg, Berlin, https://doi.org/10.1007/978-3-642-27151-9_13, pp. 505–547, (2013).

[17] Hah, C., and Lakshminarayana, B., "Measurement and Prediction of Mean Velocity and Turbulence Structure in the Near Wake of an Airfoil", Journal of Fluid Mechanics, Vol. 115, pp. 251-282, (1982).

[18] Chang, J.W., and Yoon, Y.H., "Camber Effects on the Near Wake of Oscillating Airfoils", Journal of Aircraft, Vol. 39, pp. 713-716, (2002).

[19] Ma, R., Yang, Y., Li, M., Li, Q., "The Unsteady Lift of an Oscillating Airfoil Encountering a Sinusoidal Streamwise Gust", Journal of Fluid Mechanics, Vol. 908, pp. A22, (2021).

[20] Zhu, W., McCrink, M., Bons, J.P., and Gregory, J.W., "Aerodynamic Performance and Trailing Edge Flow Physics on an Airfoil in an Oscillating Freestream", in AIAA Scitech 2020 Forum, January 6-10, Orlando, USA, (2020).

[21] Tabrizian, A., Tatar, M., Masdari, M., Eivazi, H., and Seddighi, M., "An Experimental Study on Boundary Layer Transition Detection over a Pitching Supercritical Airfoil using Hot-film Sensors", International Journal of Heat and Fluid Flow, Vol. 86, pp. 708-743, (2020).

[22] Wernert, P., Geissler, W., Raffel, M., and Kompenhans, J., "Experimental and Numerical Investigations of Dynamic Stall on a Pitching Airfoil", AIAA Journal, Vol. 34, pp. 982-989, (1996).

[23] Soltani, M., and Mahmoudi, M., "Measurements of Velocity Field in the Wake of an Oscillating Wind Turbine Blade", The Aeronautical Journal, Vol. 114, pp. 493-504, (2010).

[24] Anderson, J., Streitlien, K., Barrett, D., and Triantafyllou, M., "Oscillating Foils of High Propulsive Efficiency", Journal of Fluid Mechanics, Vol. 360, pp. 41-72, (1998).

[25] Chang, J.W., "Near-wake Characteristics of an Oscillating NACA 4412 Airfoil", Journal of Aircraft, Vol. 41, pp. 1240-1244, (2004).

[26] Satyanarayana, B., "Unsteady Wake Measurements of Airfoils and Cascades", AIAA Journal, Vol. 15, pp. 613-618, (1977).

[27] Mamouri, A.R., Khoshnevis, A.B., and Lakzian, E., "Experimental Study of the Effective Parameters on the Offshore Wind Turbine's Airfoil in Pitching Case", Ocean Engineering, Vol. 198, pp. 906-955, (2020).

[28] Koochesfahani, M.M., "Vortical Patterns in the Wake of an Oscillating Airfoil", AIAA Journal, Vol. 27, pp. 1200-1205, (1989).

[29] Goodman, S., Gunasekaran, S., Altman, A., and Medina, A., "On the Near Wake Turbulent Flow Properties of the SD7003 Airfoil", in AIAA Scitech 2019 Forum, January 7-11, San Diego, USA, (2019).

[30] Boroumand, B.B., and Mani, M., "Wake Measurements of Oscillating Supercritical Airfoil in Compressible Flow", Transactions of the Canadian Society for Mechanical Engineering, Vol. 43, pp. 112-121, (2019).

[31] Masdari, M., Seyednia, M., and Tabrizian, A., "An Experimental Loading Study of a Pitching Wind Turbine Airfoil in Near-and Post-stall Regions", Journal of Mechanical Science and Technology, Vol. 32, pp. 3699-3706, (2018).

[32] Bolinches-Gisbert, M., Robles, D.C., Corral, R., and Gisbert, F., "Numerical and Experimental Investigation of the Reynolds Number and Reduced Frequency Effects on Low-pressure Turbine Airfoils", Journal of Turbomachinery, Vol. 143, pp. 1-11, (2021).

[33] Castillo, R., and Pol, S., "Wind Tunnel Studies of Wind Turbine Yaw and Speed Control Effects on the Wake Trajectory and Thrust Stabilization", Renewable Energy, Vol. 189, pp. 726-733, (2022).

[34] Yadegari, M., and Khoshnevis, A.B., "Numerical and Experimental Study of Characteristics of the Wake Produced Behind an Elliptic Cylinder with Trip Wires", Iranian Journal of Science and Technology, Transactions of Mechanical Engineering, Vol. 45, pp. 265-285, (2021).

[35] Yang, J., Yang, H., Wang, X., and Li, N., "Experimental Study of a Gurney Flap on a Pitching Wind Turbine Airfoil under Turbulent Flow Conditions", Journal of Marine Science and Engineering, Vol. 10, pp. 1-19, (2022).

[36] Aziz, H., and Mukherjee, R., "Vortex Interaction and Roll-up in Unsteady Flow Past Tandem Airfoils", Journal of Applied Fluid Mechanics, Vol. 9, pp. 3087-3100, (2016).

[37] Mamouri, A.R., Lakzian, E., and Khoshnevis, A.B., "Entropy Analysis of Pitching Airfoil for Offshore Wind Turbines in the Dynamic Stall Condition", Ocean Engineering, Vol. 187, pp. 206-229, (2019).

[38] Kou, J., and Zhang, W., "Multi-kernel Neural Networks for Nonlinear Unsteady Aerodynamic Reduced-order Modeling", Aerospace Science and Technology, Vol. 67, pp. 309-326, (2017).

[39] Choi, C.K., and Kwon, D.K., "Wind Tunnel Blockage Effects on Aerodynamic Behavior of Bluff Body", Wind and Structures an International Journal, Vol. 1, pp. 351-364, (1998).

[40] Lian, Y., "Blockage Effects on the Aerodynamics of a Pitching Wing", AIAA Journal, Vol. 48, pp. 2731-2738, (2010).

[41] Sadeghi, H., and Mani, M., "An Experimental Wake Analysis of a Pitching Airfoil", in 7th World Conference on Experimental Heat Transfer, Fluid Mechanics and Thermodynamics, 28 June – 03 July, Krakow, Poland, (2009).

[42] Choudhry, A., Leknys, R., Arjomandi, M., and Kelso, R., "An Insight into the Dynamic Stall Lift Characteristics", Experimental Thermal and Fluid Science, Vol. 58, pp. 188-208, (2014).

[43] Worasinchai, S., Ingram, G., and Dominy, R., "A Low-Reynolds-number, High-angle of Attack Investigation of Wind Turbine Aerofoils, Proceedings of the Institution of Mechanical Engineers, Part A", Journal of Power and Energy, Vol. 225, pp. 748-763, (2011).

Nomenclature

$b_{\frac{1}{2}}$	Half-width (m)
C	Chord length of the airfoil(m)
D_s	Base diameter of the hot-wire sensor
f	Frequency of pitch oscillation (s^{-1})
k	Reduced frequency
L_s	Base length of the hot-wire sensor
L_p	Length of wire support of the hot-wire sensor
Re	Reynolds number
S	Distance from wire supports of the hot-wire sensor
S_e	Sensor length of the hot-wire sensor
$\%TI$	The percentage of turbulence intensity
t	Time (s)
T	Time-period oscillation (s)
U	Wake flow velocity (ms^{-1})
u', v', w'	Velocity fluctuation in the *x*-, *y*-, *z*-directions, respectively (ms^{-1})
$u_{r.m.s}$	Mean of squared fluctuation in the *x*-direction (ms^{-1})
$\overline{U}$	Time-averaged velocity (ms^{-1})
U_∞	Free-flow velocity at the inlet (ms^{-1})
$U_{\min}$	Minimum velocity in the wake (ms^{-1})

U_0	Velocity in the center of the wake (ms^{-1})
W_0	Velocity defect parameter (ms^{-1})
X	Stream-wise dimension of coordinates (m)
Y	Cross-stream dimension of coordinates (m)

Subscripts

r.m.s	Root mean square
∞	Free stream value at the inlet

Greek symbols

ν	Kinematic viscosity (m^2s^{-1})
α	Instantaneous angle of attack (degree)
$\bar{\alpha}$	Mean angle of attack (degree)
α_0	pitch oscillation amplitude (degree)

Abbreviations

AoA	Angle of attack (degree)
AoAs	Angles of attack (degree)
CCW	Counter-clockwise
CW	Clockwise
HAWT	Horizontal axis wind turbine
HWA	Hot-wire anemometer
HSU	Hakim sabzevari university
LDV	Laser doppler velocimetry
LE	Leading edge
LEV	Leading edge vortex
PIV	Particle image velocimetry
TE	Trailing edge
TEV	Trailing edge vortex
TI	Turbulence intensity